PALL

PALL CORPORATION
PROCESS EQUIPMENT DEVELOPMENT DEPARTMENT
CORTLAND, NY 13045
REPORT NO. 693
September 20, 1999

ADVANCED HOT GAS FILTER DEVELOPMENT TOPICAL REPORT

Reporting Period:
May 1995 through January 1999

Prepared By:
Matthew R. June
John L. Hurley (deceased)
Mark W. Johnson
4/99

DOE CONTRACT DE-AC21-95MC31215

For.
U.S. Department of Energy
Office of Fossil Energy
Morgantown Energy Technology Center
PO Box 880
Morgantown, West Virginia 26507-0880

Abstract

Iron aluminide hot gas filters have been developed using powder metallurgy techniques to form seamless cylinders. Three alloys were short-term corrosion tested in simulated IGCC atmospheres with temperatures between 925°F and 1200°F with hydrogen sulfide concentrations ranging from 783 ppm_v to 78,300 ppm_v. Long-term testing was conducted for 1,500 hours at 925°F with 78,300 ppm_v. The FAS and FAL alloys were found to be corrosion resistant in the simulated environments. The FAS alloy has been commercialized.

Acknowledgements

The authors acknowledge the advice and encouragement of our FETC Project Manager Ted McMahon. Special thanks are due to several individuals at Pall including Steve Geibel (PED) and Joe Puzo (IFP) for their guidance; William Wood (IFP) for help in the spinning and vacuum sintering of seamless cylinders; Arnold Goluboff (IFP) for the welding modules and elements; and Keith Rekczis (PED) for running experiments and for help in upgrading the exposure apparatus. Special thanks are due as well to several staff members at Oak Ridge National Laboratory; these include Peter Tortorelli, Vinod Sikka, and Jack DeVan (Ret.).

Table of Contents

List of Tables

List of Figures

1.0 EXECUTIVE SUMMARY

The prime objective of this project was to commercialize weldable, crack-resistant iron aluminide filters that will provide several years of service in advanced power generation processes. The program was highly successful in attaining these goals. Pall Corporation now has a commercially available line of iron aluminide filters and the products are being marketed internationally. In general, these filters will be used to remove particulates from the gas streams prior to entering power generation turbines.

The five tasks of the project were to (1) submit a NEPA document, (2) develop a test plan, (3) develop, qualify and test an acceptable metal filter element for resistance to corrosion in a high temperature, reducing, sulfur-bearing atmosphere, (4) develop manufacturing processes to make the metal filter elements, and (5) manufacture fifty filter elements.

Pall Corporation initially selected three iron aluminide alloy compositions from recommendations by the Department of Energy's Oak Ridge National Laboratory. The three compositions were Fe_3Al with 2% chromium (FAS modification), Fe_3Al with 5% chromium (FAL modification), and FeAl containing 0% chromium. The FAS alloy was the most successful material from the perspectives of manufacturing and corrosion resistance.

The preferred commercial form for iron aluminide filters was determined to be seamless cylinders. Pall PSS® seamless cylinders have been widely accepted as industrial filters, fabricated in stainless steel and nickel base alloys. The media choice was based on technical issues related to product uniformity, ability to be manufactured, and consistency of performance in service and acceptable cost. The technology to produce seamless filter cylinders in a number of different alloys has been used by Pall for years. Iron aluminide seamless cylinders are made using a similar process as that for the production of seamless cylinders in stainless steels and other alloys. Three important changes were necessary, however, and they are addressed in this report. To produce a high strength cylinder in iron aluminide, it was necessary to (1) tailor some processing details during the production of the filters, (2) add a compaction step for the cylinders and (3) develop an optimized sintering cycle. Hardware requirements and welding procedures were also developed.

Each of the compositions was evaluated for ductility, strength and corrosion resistance. The FeAl medium, 0% chromium, was the most brittle of the compositions with poor corrosion resistance. The FAL composition, 5% chromium, demonstrated linear time-dependent corrosion, which is unacceptable for long-term industrial use. The preoxidized FAS alloy with 2% chromium demonstrated the best performance in a high temperature, reducing, sulfur-bearing atmosphere by virtue of its impervious alumina passive layer. As a result, the fifty filter elements of Task 5 were fabricated using the FAS media.

2.0 INTRODUCTION

The development of advanced, coal fired, power generation systems such as pressurized fluid-bed combustion (PFBC) and integrated gasification combined cycles (IGCC) is an important part of the future energy strategy of the United States. This technology can economically provide high efficiency power generation with minimal environmental emissions. These advanced power generation projects are, however, dependent on the development of durable, economical high temperature filter systems. Through this project, Pall Corporation has succeeded in producing iron aluminide seamless cylinder filters that appear to meet the initial requirements.

Currently, high temperature filter systems are in the demonstration phase with the first commercial scale hot filter systems installed on IGCC units and demonstration units of PBFC systems. These filters are mostly ceramic tubes or candles and, because of their low toughness, many of these brittle filter systems fail as a result of mechanical or thermal shock. Preoxidized iron aluminide filters have the necessary combined properties of metal ductility and high-temperature corrosion resistance from the passive oxide coating.

For IGCC facilities, the major concern with using ceramic filters is an inadequate crack resistance to mechanical loads. A solution to this problem has been clearly demonstrated by the development of iron aluminide filters. They have a higher intrinsic toughness than ceramic filters and can withstand the hydrogen sulfide-bearing, high-temperature gases of these systems. The objective of this project was successfully accomplished by developing crack- and corrosion-resistant, sintered filters of iron aluminide for use in advanced power generation processes. The goal was to develop filters that will provide several years of service in advanced power gasification applications without significant filter media deterioration. This criteria has been met.

3.0 PROCEDURES

3.1 Manufacture of Seamless Iron Aluminide

3.1.1 Selection of Alloy Compositions

The three alloy compositions were chosen and modified for use in a powder metallurgy process after consulting with Oak Ridge National Lab and reviewing relevant literature [1-7]. The primary considerations for the alloys were resistance to spalling and corrosive attack in a sulfur-bearing reducing environment. The mechanical properties of the alloys at elevated temperatures were also a consideration.

Powders produced by gas and water atomization techniques were reviewed. The powders were compared for the degree of green strength after compaction and by preliminary sinterability tests. The green strength is needed during handling before the sintering operation and should increase the mechanical properties after the short sintering cycle.

3.1.2 Forming a Non-Sintered (Green) Tube

The manufacturing of the iron aluminide tubes was done using the seamless manufacturing techniques proprietary to Pall. It is not possible to form and weld a tube from a porous flat sheet of an iron aluminide because of its low ductility. The process needed some modifications to accommodate the unique characteristics of the intermetallic alloy.

To form the green tube, the required amount of iron aluminide powder was individually weighed and dispersed in a thickened water based solution. This mixture was poured into a ceramic tube that had one end sealed by tape. The other end was similarly sealed with tape and the ceramic tube was rotated at a high rate on its axis. This "centrifugal spinning" caused the iron aluminide powder to be deposited as a uniform layer on the inner surface of the ceramic tube. After the first spinning, the water-based solution was decanted to remove the excess liquid and the tube was spun again. The decanting of the excess liquid prevents to alloy from rusting during to the drying step.

The next step was to carefully dry the ceramic tube together with the inner uniform layer of iron aluminide powder. The powder layer that ultimately will be the seamless cylinder was supported and protected by the surrounding ceramic tube. This green part was held together by the residual dried thickener which acted as a temporary binder.

There were several challenges that had to be overcome in making a product out of these difficult to sinter alloys. It was found that cold isostatic compression of the green cylinders overcame many of these obstacles. The compression of the green part disrupts the oxide layer on the particles by producing shear by particle rearrangement during consolidation. It is also believed that the applied pressure results in an effective pressure at the particle contacts above the yield point and causes the particle asperities to deform and provide mechanical interlocking. Consolidation pressures were limited, to maintain the desired porosity for the filter characteristics.

In preparation for isostatic pressing each ceramic tube, with its inner layer of iron aluminide, was sealed between inner and outer rubber bladders. Pressure was readily transmitted during the isostatic compression step. Conversely, the working fluid was excluded from contacting either the ceramic tube or its inner layer of iron aluminide. The inner and outer bladders were removed and re-used. Both ends of the tubes were dipped in a thickened slurry of iron aluminide powder and were dried again. This secures the ends of the powder to the ceramic tube during the subsequent sintering operation.

3.1.3 Sintering

The iron aluminide alloys were vacuum solid-state sintered. The ceramic tubes, with their inner layers of consolidated iron aluminide powder, were placed vertically in the vacuum furnace. The furnace heat cycle was established to first pyrolyze the organic binder then heat-up slowly to provide for relatively uniform temperature throughout the load. The porous iron aluminide expanded more rapidly than the ceramic tube as the temperature was raised, therefore, a measure of support for the iron aluminide was provided as the powder compact expands into the ceramic.

The sintering load was made with the iron aluminide containing ceramics surrounded by a layer of shield ceramics. The shield ceramics reduce the thermal gradient across the sintering load. A manual pumpdown is performed prior to the initiation of the sintering program. This is done by purging the cool furnace with argon multiple times to lower to partial pressure of oxidants in the furnace.

After sintering, the tubes were cooled to room temperature under a vacuum or in argon. The iron aluminide tubes had effectively shrunk due to their expansion against the ceramic at sintering temperature and shrinkage from sintering. During cooling the iron aluminide contracts away from the ceramic because of the difference in the thermal expansion. They were, as a result, easily removed from the ceramic tubes. The ceramic tubes were used repetitively. The load was disassembled according to normal practice and ceramic cylinders and sintered filter tubes were removed from the load and marked for traceability.

3.1.4 Machining

All parts welded to the media were made from 310 stainless steel. The machinability of stainless steel is well known. There was no need to develop iron aluminide machining parameters (other than abrasive cutting and grinding) because the welding of the iron aluminide tubes to 310 stainless steel was successful.

Some modifications were needed in the handling and cutting procedures of the iron aluminide porous media. These were mainly focused on reducing the possibility of the media to be contaminated by other alloys at Pall.

3.1.5 Welding

Tubes that were made into filter elements for corrosion tests were prepared by cutting them to length using an abrasive cutoff wheel, squaring off using a disc grinder, and deburring the ends using a wire wheel.

The welding of the hardware to the iron aluminide was accomplished using a tungsten inert gas (TIG) welding process. 310 stainless steel was welded directly to the media with a 310 stainless steel filler (see Figure 1). Argon was used as the shield gas and as a backup gas inside the element. No pre- or post-weld heating was necessary to form an acceptable weld with the 310 stainless steel filler. The preoxidation of the media may relieve some of the welding stress.

3.2 Short-term Exposure Tests

3.2.1 Corrosion Test Apparatus

A three zone, 4.0 inch diameter, 36 inch long solid tube furnace was used for the elevated temperature exposure testing. This furnace was linked to a second, 3.0 inch inside diameter, 24 inch tube furnace for preheating the simulated IGCC atmosphere.

The muffles for the furnaces were made of Alonized stainless steel, a preferred containment material for atmospheres that have hydrogen sulfide as a constituent. Both furnaces were operated horizontally. Temperature uniformity was favored by this positioning. The length of the uniform zone in the 4.0 inch diameter furnace was maximized to contain the four test filter elements. The tube that spanned the gap between the two furnaces, containing the simulated atmosphere, was insulated to reduce the loss of heat.

The four filter elements were attached end to end, with the final element blinded off, via the threaded hardware to make a "flow through" assembly for short-term exposures one through five. A graphite antisieze tape (Grafoil) was used on the NPT fittings to keep the individual test filters from galling and to make sure that the filter string could be disassembled after 1, 3, 7, and 14 days of cumulative exposure for non-destructive property testing. The string was then reassembled using the Grafoil tape. The filters were rotated in the filter string, as is common practice in corrosion testing. A support was inserted between the second and third filters in the string to avoid creep during exposure.

For temperature monitoring, two thermocouples were placed in the center of the hot zone length. One was inside the filter string while the other was on the outside. The thermocouples were connected to a strip chart recorder providing a continuous record of temperature versus time.

3.2.2 Blowback Testing

Thermal pulsing was added to the exposure test to check the iron aluminide alloy candidates for susceptibility to spalling the oxide scale. Timed solenoid valves controlled the thermal pulsing. The following pulse parameters were chosen to simulate typical service conditions during blowback of filters:

Pulse Duration = 0.75 s
Pulse Frequency = every 15 min
Velocity = 18 ft/min
Pulse gas = Nitrogen
Pulse Temperature = Room Temperature

3.2.3 Test Atmosphere

The atmosphere consisted of a mixture of hydrogen, carbon monoxide, methane, hydrogen sulfide and steam with sodium chloride, potassium chloride and hydrochloric acid. **Table 1** lists the operating conditions for representative oxygen blown (Tampa Electric) and air blown (Sierra Pacific) IGCC atmospheres at system pressure. This table also lists the test atmosphere (without nitrogen) that was used, at approximately one atmosphere, to simulate both the oxygen blown and the air blown installations. The composition for this simulation atmosphere was determined by Oak Ridge National Laboratory (see Appendix III, **Table 11 - Table 13**). The face velocity chosen was 0.5 feet per minute in forward flow. During thermal pulsing, the velocity was 18 feet per minute. The furnace atmosphere flowed from the outside to the inside of the test filters, which simulated industrial use. The simulated atmosphere was mixed in the process tube, flowed through the filters and then exited the furnace.

Hydrogen, carbon monoxide, carbon dioxide and methane were dispensed from individual pressurized cylinders. A reservoir filled with DI water plus NaCl, KCl, and HCl supplied the water and chlorides to the test stand. Hydrogen sulfide (H_2S) was dispensed from a tank (liquid phase). Provisions were made to measure the hydrogen sulfide levels before and after the gas passed through the filter string. Each day the H_2S level was monitored at the inlet and at the outlet of the furnace tube. To measure the H_2S levels a Toxic Gas Detector Model 8014KA (Matheson-Kitagawa) was used. The H_2S inlet and outlet ports were connected in a tee, this allowed the gas to be flowing while the H_2S was being measured. The hydrogen sulfide level outlet was kept within 15% of the target level. The hydrogen sulfide was scrubbed from the gas using a 10 wt% solution of sodium hydroxide.

3.2.4 Test Procedure

The qualification of the iron aluminide porous media samples was done using both non-destructive and destructive testing. Corrosion testing was accomplished by exposing the samples to the simulated IGCC atmosphere at increasing time intervals. The samples were removed after 1, 3, 7, and 14 days of cumulative exposure. This allowed the progress of the samples to be monitored. The samples were non-destructively tested as described in section 3.5.1 during each shutdown of the cyclic testing. At the conclusion of the exposure run and after the last non-destructive tests, the filters were cut into samples for destructive testing as described in section 3.5.2.

Four filter samples were exposed in each fourteen-day experiment. One sample of each alloy (FAS, FAL, FAS-0% Cr) was preoxidized for each test. The last sample was an as-sintered FAS alloy. This allowed the effect of the preoxidation to be assessed.

Two additional exposure runs were conducted outside of the contract with the Department of Energy. Exposure Runs 5 (1050°F with 0.0783 vol% H_2S) and 6 (1200°F with 783 vol% H_2S) are included in the report to fully disclose all of the exposure testing conducted at Pall of the iron aluminide alloys in IGCC conditions. Exposure Run 6 was used to evaluate the iron aluminide media in severe conditions, observe the effect two preoxidation temperatures (800°C and 1000°C), and qualify a new set of removable hardware. It is known that the preoxidation forms a transitional alumina and temperatures in excess of 950°C are needed to form an alpha-alumina. The alpha-alumina is superior to the transitional alumina with respect to slower parabolic growth and corrosion resistance. Short-term exposure run six was done using the removable hardware design for the long-term exposure test.

3.3 Long-Term Exposure Test

Long-term exposure testing was conducted using the same equipment as the short-term exposure tests with a few minor modifications. The solid fixturing for holding the exposure samples was altered to remove the mass of the 310 stainless steel hardware from the mass gain measurements done at each cyclic exposure interval. The hardware was not welded to the porous metal samples. A rough seal was made between the samples and hardware by placing them in compression using a tie rod (Figure 2). This method allows the removal of the hardware at each interval by sacrificing a hermetic seal. This allowed some bypass of the filter media at the junction of the media and hardware. The filter samples were rotated in the filter string, as is common practice in corrosion testing.

Only the FAS and FAL alloy compositions were evaluated in the long-term corrosion test. The FAS-0% Cr alloy was eliminated based on welding problems, poor mechanical properties, and inferior corrosion resistance with respect to the other two alloys. All the samples were preoxidized to form a continuous alumina layer. The long-term exposure conditions were the same as short-term exposure Run 3 (925°F with 7.83 vol% H_2S at 1 atm).

Three sets of FAS and FAL preoxidized samples were exposed; two sets were placed in the test stand at one time. The samples were removed for non-destructive testing at 31, 62, 125, 250, 500, 750, 1000, 1250, and 1500 hours of cumulative exposure. One of the first two sets of exposure samples was removed after 500 hours of exposure and replaced with the third set. This resulted in three exposure lengths of 500, 1000, and 1500 hours for destructive testing and evaluation.

3.4 Manufacture of Fifty Filters

The manufacture of fifty 1.5 meter long iron aluminide filters was done at the request of the Department of Energy. This served to demonstrate that Pall had the capabilities to produce small quantities of industrial scale elements. The elements were sent to the Sierra Pacific Power / Pinon Pine facility in Sparks, Nevada; and the Dynegy Power Corporation plant in Terre Haute, Indiana and will be analyzed post-exposure to determine the performance of the media in actual service conditions.

3.5 Property Testing

3.5.1 Non-Destructive Tests

3.5.1.1 *Mass*

The mass of the iron aluminide media for short-term exposures one through five was determined to ±0.01 grams on a Denver Instrument model 3100XL scale. The short-term exposure samples masses included the iron aluminide media with the stainless steel end caps and filler metal. The mass of short-term Exposure Run 6 and long-term exposure samples were determined to ±0.0001 grams using a Mettler AE200 scale. These did not include welded fittings.

3.5.1.2 *Pressure Drop*

The pressure drop in inches H_2O across the filter media was recorded at a flow of 28 acfm/ft^2.

3.5.1.3 *Bubble points [8]*

Samples were wet in Filmex-B (denatured ethyl alcohol) and submerged approximately half inch below the surface prior to testing. Stoppers were placed in the open ends of the samples. Air pressure inside the element was gradually increased. The pressures at which the first and tenth bubbles occurred were recorded. The first bubble point is the pressure at which a bubble of air escapes from the largest pore in the sample: it can be correlated to the absolute filter efficiency. The tenth bubble point can be compared against the first bubble point to judge the uniformity of the pore size.

The open bubble point was also recorded. The open bubble point is an indication of the pressure required to pass a specified quantity of air (1 scfm/ft^2) with the element wet in Filmex-B and relates, by experience, to the average pore size. The equations below are for calculating the pore size are provided.

$$d = \frac{4\gamma}{\Delta p}$$

$$\Delta p = p_0 - p_1$$

$$p_1 = 9.81 \times \rho_1 \times h$$

d= pore throat diameter in meters
γ= surface tension of liquid. (Filmex-B = 0.0234 N/m)
p_0= gas pressure in Pascals. (1 inch of water = 248.84 Pa)
p_l= pressure of the liquid at the level of bubble formation.
ρ_l=density of the test liquid. (~ 780 - 850 kg/m^3)

The pore size calculated from these equations is a rough estimate used for quality control. The exposure conditions could potentially alter the surface interaction of the Filmex-B and media causing unaccountable variations of the bubble points over the exposure conditions.

3.5.1.4 *Visual Inspection*

During each stage of testing, the filters were examined visually. Any abnormalities or changes in filter appearance were recorded.

3.5.2 Destructive Tests

3.5.2.1 *Carbon/Sulfur*

A calibrated (NIST traceable standard) LECO CS-2 Carbon/Sulfur Determinator Model 788-000 was used to measure the carbon and sulfur contents of the short-term and manufacturing optimization samples. A calibrated (NIST traceable standards) LECO Model CS444 Carbon/Sulfur Determinator was used for the long-term exposure samples.

3.5.2.2 *Oxygen/Nitrogen*

A LECO TC-436 Determinator was used to measure the oxygen and nitrogen contents of the samples, tested in accordance with ASTM E 1019-94.

3.5.2.3 *Chromium*

A Metorex Energy Dispersive X-Ray Fluorescence unit was used the measure the chromium level of the samples. The Metorex X-Met 880 EDXRF on program model #4 (Low ID) with the analysis time increased to 200 seconds took three readings and then they were averaged. The Metorex X-Met has an accuracy of ± 9%.

3.5.2.4 *D-Ring Tensile Test*

Half-inch tall rings were used to test each element in a D-ring tensile testing apparatus (see Figure 3). The D-ring tensile test, while acceptable for ordinary stainless steels, requires a substantial amount of deformation before the test ring is in full contact with the D-ring supports. This amount of deformation can lead to premature failure of less ductile materials, such as iron aluminides.

3.5.2.5 *Ring Burst Strength Test*

The ring burst test places the one-inch tall sample under tension, until failure by compressing a putty that is placed inside the ring (Figure 4). This test removes any alignment and ductility factors that are associated with the D-ring tensile test, the typical method of measuring the strength of a cylindrical specimen.

$$\sigma = P\frac{r_1^2 + r_0^2}{r_1^2 - r_0^2}$$

σ = Modulus of rupture
P = Pressure on putty at fracture
r_1 = outer radius of test ring
r_0 = inner radius of test ring

3.5.2.6 *Ductility (Ring Crush Test)*

The ductility of each sample was determined using the ring crush test. The ring crush test was performed using a vise and a 0.50-inch tall ring cut from the element. The ring was placed in the vise bringing the jaws barely in contact with the test ring. The separation of the jaws was measured, with no deformation of the ring at this point. The vise was slowly closed until the ring exhibited gross cracking. The separation of the vise jaws was then re-measured. The ratio of the change in the separation of the vise jaws to the original distance is used as a relative measurement of ductility.

3.5.2.7 *Pore Distribution*

The pore size distribution was determined using mercury porosimetry using Autoscan-25 and Autoscan-60 mercury porosimeters. This will give the overall pore distribution qualitatively.

3.5.2.8 *Surface Area*

The multipoint BET surface areas are determined on an Autosorb-I sorptometer.

3.5.2.9 *Scanning Electron Microscope Examination*

Sections of media were examined with an Amray 1830T digital scanning electron microscope (SEM) and a Princeton Gamma-Tech x-ray spectrometer with digital image processing. Cross-sections were mounted in black epoxy fine powder and carbon-flashed to reduce charging. Fracture samples were mounted in the SEM with alligator clips. Robinson backscatter mode of signal detection was used. Qualitative analysis of the samples was done using energy dispersive spectroscopy (EDS). Quantitative analysis of the samples was not performed because the material did not satisfy the requirements for bulk samples.

4.0 RESULTS AND DISCUSSION

4.1 Manufacture of Seamless Iron Aluminide

4.1.1 Selection of Powder Compositions

Three compositions of iron aluminide powders were selected in the Fe_3Al region of the iron-aluminum phase diagram. These were the FAS, FAL, and FAS-0% Cr and the compositions of the powders as-produced by the manufacture are listed in **Table 3**. The composition of the alloys deviates from the typical chemistry of cast or wrought iron aluminide alloys. Boron was not added to the FAS or FAL version and the FAS and FAS-0% Cr had the same amount of zirconium as the FAL.

The iron aluminide powders were air-induction melted and water-atomized by Ametek Specialty Metal Products (Route 519, Eighty-Four, PA 15330). The powders were sieved to a −100 +325 standard mesh powder cut. Approximately 5-10 wt% of the powder was allowed to fall outside the sieve cut to keep the powder cost at an acceptable level. This is typical of powders used in porous metal filters.

The mechanical properties of the FAS alloy improved with increasing sintering temperature (**Table 5**). The elevated sintering temperatures did not appear to markedly affect the pressure drop of the media. This is expected within the small sintering temperature range because of the particle geometry and open pore structure. The results for the FAL and FAS-0% Cr alloys also indicate benefits from higher sintering temperatures. However, there were not enough samples created to confirm the effect. The media properties for the various sintering trials are contained in **Table 6 - Table 8.**

4.1.4 Machining

The machining characteristics of the iron aluminide are similar to other porous metal media. Typically, the iron aluminide media is cut with a diamond blade in an abrasive cutoff saw. Then the edges were squared-off with a disc grinder, then deburred with a wire wheel. The cut edges were then finished with a diamond files. The cutting blades, wire wheels, abrasive discs for the grinder, and files are used exclusively for the iron aluminide tubes to avoid cross contamination from nickel bearing alloys.

4.1.5 Welding

A skilled welder can reliably weld FAS and FAL versions of iron aluminide porous media to the solid joiner ring. There is more art than science in the welding of porous media. The joiner rings are typically 310 stainless steel. Other alloys can be used to provide additional hardware corrosion resistance in aggressive atmospheres.

The FAS-0% Cr alloy commonly exhibited cracking after welding. One sample in the short-term exposure testing (T-43-7, run 4) broke during the first day in the heat affected zone. The FAS-0% Cr problems with welding caused more work to be focused on the FAS and FAL versions.

4.2 Short-Term Exposure Tests

During the exposure runs, two of the iron aluminide samples mechanically failed in the test stand. These were attributed to the difficult nature of and inexperience with welding the porous media. The initial FAL sample in exposure number two failed during the first day. It was replaced with a new FAL sample, resulting in a FAL sample with only 312 hours (13 days) of exposure opposed to the typical 336 (14 days). The FAS–0% Cr sample in exposure number four failed during the first day of testing. It was not replaced, there was no media immediately available. Both failures occurred in the heat affected zone.

A SEM examination was not conducted on the exposure run five samples. The exposure conditions (1050°F with 0.0783 vol% H_2S) and non-destructive results did not warrant the effort to fully examine the samples after exposure. Two samples the FAS–0% Cr and FAL, were not burst tested. The piston seals for the burst test would not seal properly with the sample.

4.2.1 Non-Destructive Test Results and Discussion

4.2.1.1 *Mass*

The plots of mass gains for short-term Exposure Runs 1-6 are included as Figure 5 - Figure 11. The mass gain of the alloys during the short-term exposures one through five includes the corrosion of the solid 310 stainless steel hardware and soot deposition. Exposure Run 6 was accomplished with removable hardware. The soot was partially removed during each non-destructive evaluation of the cyclic testing because the samples were submerged in Filmex-B. The 310 stainless steel corrosion, soot deposit, and the iron aluminide media corrosion mass gains are impossible to separate with the data gathered.

Generally, the FAS non-oxidized samples exhibited mass gain rates exceeding the other samples. This indicated that the preoxidation to form the continuous layer of alumina is beneficial to the iron aluminide porous media or the alumina formation on the non-oxidized sample had a marked influence on the mass gain. Alumina can form in very low partial pressures of oxygen in atmospheres similar to the simulated IGCC tests. However, the rate of formation may be slow enough to allow some attack of the media on a non-preoxidized sample. This is also coupled with the fact that the filter media has a high surface area resulting in competition for the available oxygen for alumina formation.

During Exposure Runs 2 and 3, the 310 stainless steel was noticeably spalling. The corrosion product was not identified; nickel sulfide formation was suspected. The spalling of the hardware affected the mass gains of the iron aluminide samples. The mass gains measured during these exposures are very low for a porous metal media in these conditions. It is known that a stainless steel and many chromia-forming superalloys can not be operated in these conditions as a porous media.

The mass gains for Exposure Run 6 demonstrated the dramatic difference between the 800°C and 1000°C preoxidation temperatures (see Figure 10). The 1000°C samples had a much greater rate of mass gain than the 800°C samples. It is clear that alpha-alumina was not formed on the 1000°C preoxidized samples and the 800°C preoxidation is an effective diffusional barrier for the present FAS and FAL alloy compositions. The 800°C preoxidized samples mass gains are plotted on a separate chart so the relationship between the FAS and FAL sample can be made (Figure 11). The FAS alloy appeared to have a slightly higher rate of mass gain. However, the differences are extremely small and could be affected by small interactions with the removable solid hardware. Both alloys are equivalent in this severe atmosphere.

To elucidate the performance of the FAS and FAL alloys with respect to the severity of the different test atmospheres, the mass gain curves are compared per alloy on separate charts (Figure 12 and Figure 13). Both charts demonstrate that the alloys were affected more by hydrogen sulfide content then by temperature. The affect of the 310 stainless steel hardware can be found by observing that Exposure Run 6, the most severe condition, is not the highest on the charts. Other Exposure Runs (2,3 and 4) have mass gains that are much more affected than Exposure Run 6. The mass gains of all of the exposure runs should be below that of Exposure Run 6 if the effect of the 310 stainless steel hardware could be removed.

The life expectancy of the iron aluminide media can not be accurately predicted from the short-term exposures. Alloys that are corrosion resistance tested in an environment will eventually reach a state during exposure where the rate of mass gain slows significantly. It is not believed that the short-term exposures were long enough to allow the iron

aluminide media to reach this point. Any extrapolation of the short-term data would result in a premature failure prediction.

4.2.1.2 *Pressure Drop*

The plots of pressure drop changes for short-term Exposure Runs 1 through 6 are included as Figure 14 -Figure 20. It is expected that there will always be an increase in pressure drop after an exposure. For the IGCC filter applications the pressure drop of the filter will be dominated by the permanent filter cake that is formed by the ash during the initial stages of filtration. A major increase in pressure drop of the filter media indicates the media is blinding.

In general, the FAS-0% Cr alloy had the largest increase in pressure drop of all of the samples. This is clearly evident when the raw data (**Table 14 - Table 19**) is inspected to examine the pressure drop increases after the samples were ultrasonically cleaned in IPA. Upon cleaning there is fifty percent reduction in the increase of the pressure drop, approximately. This is from the removal of the carbon soot that was deposited in the pores during exposure. All of the pressure drop increases, with the exception of some in Exposure Run 6, are considered acceptable and do not indicate any degradation in filtration performance.

The 1000°C preoxidized samples in Exposure Run 6 had a major increase in pressure drop. This indicated that the media was being adversely affected by the exposure conditions. The FAS and FAL 1000°C samples had pressure drop increases of 1480 and 308%, respectively. The 800°C preoxidized FAS and FAL samples had pressure drop increases of 7 and 11%, respectively. The 800°C sample pressure drops are acceptable while the 1000°C samples are not.

The comparison of the FAS and FAL samples from the short-term exposure runs reveals the general trend of increasing pressure drop over time. This is the expected result because of the carbon soot deposition on the surface of the media. The pressure drop could also increase if there was a corrosion product formation that constricted the pores or caused an increase in turbulence. These would be very subtle and rarely detectable. Neither is detrimental to the media. The marked increase of the pressure drop of the 1000°C preoxidized samples should serve as an example of corrosion detection via pressure drop measurement.

4.2.1.3 *Bubble Points*

The bubble points of the exposed iron aluminide media should only be used as a guide to media performance. The surface energy, and hence the wetting angle, of the media can be changed by the exposure conditions.

The open bubble points (Figure 23 -Figure 28) had a fluctuated within a ±10% range of the samples original values, with the exception of the 1000°C preoxidized samples from Exposure Run 6. These are minor changes and do not indicate any corrosion or other degradation of the media. The 1000°C preoxidized samples from Exposure Run 6 had open bubble point increases of 77 and 47% for the FAS and FAL compositions, respectively. These increases indicate the closure of pores and a strong possibility of corrosion.

The comparison of FAS (Figure 29) and FAL (Figure 30) open bubble points per alloy in the six different exposure conditions demonstrates that the fluctuations are typical for the media in all exposure conditions. It appears that the open bubble points will eventually reach a stable point in these exposure conditions. This could only be confirmed by longer exposures and is unnecessary because this experiment does not examine the effect of the

ash and char on the samples that would occur in actual filtering conditions. The ash and char will affect the media bubble points, probably causing an increase.

The first (Figure 31 - Figure 38) and tenth (Figure 39 - Figure 46) bubble points of the media during the exposures do not follow any clear trends. The method of data collection is too subjective to be of any substantial use in evaluating the very minor changes in the iron aluminide media during exposure. If a different metal media (perhaps 310 stainless steel) was tested with the iron aluminide media the comparison of the results would reveal that the iron aluminide alloys are very stable. However, without a "control" the data appears to be random.

4.2.1.4 *Visual Inspection*

The as-sintered media was a dark gray color. After preoxidation, the media color is a varied "oil slick" color. This is because of variations in the thickness, from epitaxial growth, of the thin oxide film causing different levels of interference. After each exposure cycle, the samples would be covered in black soot. This soot could be smeared but remained on the filter after bubble pointing in Filmex-B. The 1000°C preoxidized FAS and FAL samples developed metallic spots on and in the media. This was a clear indication of corrosive attack.

4.2.2 Destructive Tests

The destructive test results for short-term Exposure Runs 1-6 are contained in **Table 9.** Some ring burst data points are missing. Samples were not available for testing or the sample was cracked prior testing.

4.2.2.1 *Carbon/Sulfur*

The carbon levels for all the short-term exposure samples did not show significant change. The carbon values for the exposed samples were within the range currently accepted for the manufacturing of iron aluminide. The carbon level of the iron aluminide has not been affected by the exposure

The sulfur levels of the samples from Exposure Runs 1-5 have slightly increased. The increase in sulfur is generally proportional to the increase in hydrogen sulfide content of the test atmosphere. The increases are low and are not considered detrimental to the performance of the filter or an indication of sulfidation of the iron aluminide media. The exact disposition of the sulfur is unknown.

The Exposure Run 6 samples that were preoxidized at 800°C had a mild increase of sulfur level. The FAS sample had a 0.0711 wt% (756%) increase and the FAL sample had a 0.0689 wt% (689%) increase. The deposition of sulfur in the pores of the aluminum oxide on the surface of the iron aluminide and the formation of small sulfides caused this increase. This has been indicated by Auger Electron Spectroscopy (AES), conducted outside of this testing. The sulfur is generally contained in the first 0.25 μm of the material; the first 0.50 μm of the material is the alumina layer. AES analysis was not conducted on these samples.

The Exposure Run 6 samples preoxidized at 1000°C had a major increase in sulfur content. The FAS sample had an increase of 1.5256 wt% (16229%) and the FAL sample increased by 0.9394 wt% (9394%). This amount of sulfur indicates the formation of sulfides.

4.2.2.2 *Oxygen/Nitrogen*

The oxygen/nitrogen measurements indicate that the media had a small increase in oxygen during exposure. The partial pressure of oxygen for alumina formation is very

low. It is reasonable to assume that the alumina oxide continues to slowly grow during the exposures. The increases in oxygen are beneficial, in reducing conditions, to the corrosion resistance of the iron aluminide alloys. There was no measurable change in the nitrogen content of the samples. This is to be expected. Nitrogen is only briefly present as the thermal backpulse.

4.2.2.3 *D-Ring Tensile Test*

The D-ring tensile test results are inconsistent. This was discovered during the development of the iron aluminide sintering profile. Premature failures occur because the rings need to be bend around the D-rings before the test becomes mainly tensile. Iron aluminide porous media does not have enough ductility to consistently fully contact the rings for proper testing. Most failures occurred prior to the iron aluminide fully meeting with the D-rings. The putty ring burst test, typically used for ceramics, proved to be more consistent.

4.2.2.4 *Ring Burst Strength Test*

The ring burst results for the first four exposure runs do not have any controls. This does not allow a direct comparison to be made for the loss of strength over time for these exposure conditions. However, judging by the strengths measured after exposure and the strengths of the media being produced at the time of sample production, the strength of the media does not seem to have been significantly reduced.

The FAS samples from Run 5 had decreases of 50% and 55% for the oxidized and non-oxidized samples, respectively. The magnitude of the decrease was unexpected. However, it is unknown when the decrease in strength occurred. The assumption of linear decay of strength for a porous metal media can be very hazardous. A majority of the strength loss could have occurred during the first hours of testing. These test results are confusing when compared to Exposure Run 6 and the long term exposure results that indicate a minor loss of strength in more severe conditions.

The strength of the FAS Exposure Run 6 samples increased as the oxidation temperature increased for the unexposed samples. The strength of the FAS samples increased by 77% and 100% when preoxidized at 800°C and 1000°C, respectively. The FAL alloy strength varied with the preoxidation temperature. The FAL sample preoxidized at 800°C lost 12% of its strength while the samples preoxidized at 1000°C increased by 25%. Preoxidation of the FAS alloy has a positive effect while the effect on the FAL alloy is undetermined.

The exposed exposure run six FAS sample, preoxidized at 1000°C, could not be tested using the ring burst test because of a longitudinal crack in the media. It is believed that this sample was dropped before exposure testing began. The exposed samples decreased in strength, the FAS sample preoxidized at 800°C retained 74% of it strength. The FAL samples retained 34% and 47% of their strength for the 800°C and 1000°C preoxidations, respectively. It is believed that if the FAS sample preoxidized at 1000°C could be tested, it would have exhibit significant strength loss.

4.2.2.5 *Ductility (Ring Crush Test)*

The ductility of all samples decreased with exposure. This is common for other porous metal media after exposure. The ductility results are only qualitative. A comparison between the exposure tests is not recommended.

4.2.2.6 *Scanning Electron Microscope Examination*

The SEM images are contained in appendix V (page 82).

4.2.2.6.1 Control Images

The iron aluminide powder utilized for the production of the porous metal media was water-atomized. The images (Figure 58 and Figure 59) demonstrate the irregular surfaces that provide a high green strength. The green strength is obtained by a combination of mechanical interlocking from the deformation of asperites and friction between particles. The mechanical interlocking allows the sintering of the alumina forming alloys. The surfaces of the iron aluminide particles are free of most contaminants. However, it is reasonable to assume that the particles are covered in a well-adhered layer of alumina.

The surfaces of the as-sintered iron aluminide particles have light and dark nodules that are approximately one micron in size (Figure 61 - Figure 62). The light nodules have been identified as zirconium (Figure 65), which is likely in the form of an oxide. The zirconium has diffused to the surface of the iron aluminide particles during sintering. The darker nodules are alumina (Figure 66), probably formed from pure aluminum during cooling of the sintering load. The aluminum may be deposited on the surface of the particles from aluminum removed from the alloy because of the high aluminum vapor pressure, deposition can occur during cooling after sintering. This is similar to the removal of chromium from a stainless steel that is common in solid state vacuum sintering.

The control samples for Exposure Runs 1-4 (Figure 67 - Figure 72) images show a homogenous media. These controls were not preoxidized. The spectra collected are through the epoxy layer of the surface of the particles. These images are typical for the iron aluminide media. SEM analysis of the samples for Exposure Run 5 was not conducted.

The control samples for Exposure Run 6 are contained as Figure 73 - Figure 99. The samples were preoxidized prior to the examination. The FAL samples were manufactured from a mixture of gas-atomized and water-atomized powders. The FAL media will contain irregular particles with spherical particles. The cross-sections of the FAS and FAL samples (Figure 73 - Figure 82) revealed the typical features of the iron aluminide porous media, There were some dark and light inclusions in the base metal, these are alumina and zirconia inclusions, respectively. The FAL sample preoxidized at 1000°C had some dark pools on the particle surface (Figure 81). The dark pools were identified as a mixture of aluminum and zirconium (Figure 82), most likely oxides.

The upstream surfaces (outer diameters) of the media were examined for the Exposure Run 6 samples. The 800°C preoxidized samples (Figure 83 and Figure 86) are typical for the iron aluminide media. The gas-atomized particles of the FAL samples can be seen mixed with the water-atomized particles. The some of the FAL sinter bonds were fractured, this explains the lower burst strengths of the FAL media used for Exposure Run 6 compared to that manufactured with all water-atomized powder. The 1000°C preoxidized samples (Figure 87 - Figure 90) have a different surface morphology than the 800°C preoxidized samples. The nodules are more pronounced and the surface texture on the gas-atomized particles appears rougher. The higher preoxidation temperature definitely affects the iron aluminide in a different manner. The fractured samples (Figure 91 - Figure 99) have the same surface morphologies as the upstream samples. The fractures of the iron aluminide are typically transgranular and brittle.

4.2.2.6.2 Exposed Samples from Run 1 – Run 4

Exposure Runs 1-4 were analyzed with the SEM using cross-sections only. The cross-section images (Figure 99 –Figure 128) were collected in the center of the samples and the spectra were collected through the epoxy layer of the particle surface. The were no signs of the corrosion found on the samples, with the exception of the FAS non-oxidized sample of Run 4 (T-42-9). There was a fine layer on the surfaces of the some of the particles. It is not clear what the layer is composed of or why it was only detected on this sample. The layer does not appear to affect the base metal, it is not believed to be detrimental to the iron aluminide media.

4.2.2.6.3 Exposed Samples from Run 6

4.2.2.6.3.1 FAS alloy preoxidized at 800°C, exposed

The FAS alloy preoxidized at 800°C has formed metal sulfides on the outer surface of the media. The sulfides can be seen in Figure 142 and Figure 143 as the faceted crystal structures on the surface. The sulfides have just begun to coarsen after fourteen days. The small crystals will eventually grow into one another to form larger crystals. This growth would lead to plugging of the elements, if the sulfidation continues. Sintering followed by preoxidation may leave free iron on the surface of the alumina scale. This free iron would be easily sulfidized and depleted rapidly. The cross sections (Figure 129 and Figure 130) of the media did not indicate that the base metal was affected. The continuous alumina layer should prevent the diffusion of sulfur into the base metal. Without attack of the base metal the media should not be detrimentally mechanically affected. The formation of sulfides may degrade the filter properties of the media.

The sulfide crystal formation was limited to the upstream surface, the fractured surface images (Figure 150 and Figure 151) do not indicate any sulfidation. A full screen EDS spectrum of the image at 2000X did not detect sulfur. The fracture surfaces of the exposed material are similar to the control fracture surfaces (Figure 91 and Figure 92).

4.2.2.6.3.2 FAL alloy preoxidized at 800°C, exposed

The upstream surface has been sulfidized, small faceted crystals have formed over the entire surface (Figure 142 and Figure 143). There appears to be a higher concentration of crystals on the water-atomized powder than the gas-atomized powder; this could be related to surface energy and available surface area. The cross-section images (Figure 131 and Figure 132) demonstrate that the sulfides are formed only on the surface of the media and are not affecting the base metal. The continuous alumina scale is preventing the diffusion of the sulfur into base metal.

The orientation and morphology of the corrosion product's crystal structure is different between the FAS (Figure 143) and FAL (Figure 145) alloys. The crystals on the FAS alloy are almost all "attached" to the iron aluminide with the large hexagonal plane while the crystals on the FAL alloy generally are "attached" by the smaller rectangular sides.

The fracture surface of the FAL alloy, preoxidized at 800°C, (Figure 152 and Figure 153) is very similar to the control (Figure 93 and Figure 94). The mixing of the gas- and water-atomized powders can be clearly seen. The fracture of the FAL alloy reveals a porous sinter bond. Porous sinter bonds have occasionally been seen in the FAS alloy but not in the concentrations seen in the FAL. Porous sinter bonds reduce the mechanical properties of the media.

4.2.2.6.3.3 FAS alloy preoxidized at 1000°C, exposed

The 1000°C preoxidation was detrimental to the corrosion resistance of the FAS alloy. The fracture surface of the alloy (Figure 154 and Figure 155) was dominated by flakes that are believed to be composed of a mixture of alumina and iron sulfides; a more detailed analysis is needed to be certain. Flakes like this form by a tube (a 50-100 angstroms in diameter) in the center of the flake transporting the elements to the top of the flake for reaction with the atmosphere allowing growth [9]. The tube will penetrate the oxide layer into the base metal allowing the iron to diffuse to the surface to form sulfides. Eventually, voids will form and the corrosion product will spall off the particles.

The upstream surface of the FAS alloy (Figure 146 and Figure 147) was covered with similar flakes and some larger crystals. The large crystals are composed of mainly aluminum and zirconium with oxygen. This is a mixed oxide formed by the zirconium on the surface (the zirconium in the alloy diffuses to the surface of the particles during sintering) and the aluminum competing for the oxygen during preoxidation. The free energy of formation of alumina (Al_2O_3) and zirconia (ZrO_2) are extremely close at 1000°C. The zirconia has the lower free energy and will form before alumina. This is opposite of what occurs with an 800°C preoxidation. The oxides are growing in the reducing conditions.

The cross-section (Figure 134 and Figure 135) illustrates why the pressure drop of the samples was extremely high. The entire outer surface of the samples was sealed with a mixture of the sulfide flakes and mixed oxides. Spectra for the different areas in Figure 135 are provided in Figure 136 thorough Figure 138.

4.2.2.6.3.4 FAL alloy preoxidized at 1000°C, exposed

The type of attack on the FAL 1000°C preoxidized alloy is very similar to the FAS 1000°C preoxidized alloy. The fracture and upstream surfaces of the media (**Figure 156**, **Figure 157**, **Figure 148**, and **Figure 149**) are covered with the iron-, aluminum- and sulfur- containing flakes. It appears that the flakes do not form as readily on the surface of the gas-atomized particles as they do on the water-atomized particles. The upstream surface has some iron sulfide crystals growing.

The cross-section (**Figure 139** and **Figure 140**) has some gray areas on the interior of the sample. The gray area is composed mainly of alumina with some sulfur. The sulfur has probably diffused into the alumina.

4.3 Long Term Exposure Test

Three sets of iron aluminide samples were used for the long-term testing. Sample set #1 was exposure for the first five hundred hours, set #2 was exposed for the last one thousand hours, and set #3 was exposure for the full one thousand five hundred hours.

4.3.1 Non-Destructive Test Results and Discussion

4.3.1.1 *Mass*

All of the iron aluminide samples had an increase in mass. The plot of the mass gains (**Figure 158**) demonstrates that the FAS and FAL alloys perform similarly. FAL sample #1 has a marked increase after thirty-one hours of testing. This was due to a plastic spacer, used to align the filter samples in the test jig, accidentally being left in the jig during testing. If the mass gain due to the plastic were normalized to the mass gain of the other three samples, the rest of the curve would follow the other three.

The FAS and FAL sample #3 had a marked increase in mass until 500 hours testing had been completed. This increase in mass is due to the formation of iron sulfides on the upstream surface. The iron sulfides are not believed to be from the base metal, see section 4.3.2.7. Once all of the material available for sulfidation had reacted with the gas stream the mass gain rate significantly decreased. The total percentage mass gain for the iron aluminide samples exposed for 1,500 hours were 0.39% and 0.38% for the FAS and FAL alloys, respectively. After the filter samples were cleaned, they had a total mass gain for 0.31% and 0.29% for the FAS and FAL alloys, respectively. This is a remarkably low mass gain for a porous metal filter with a total surface area between 5.6 and 6.9 m^2, see section 4.3.2.6. The reduction in mass after the ultrasonic cleaning is due to the removal of soot.

Sample #2 of the FAS and FAL alloys did not show the same rate of mass gain as the other samples. These samples are from a different sintering and preoxidation batch. There are probably slight differences in the sintering and preoxidation of the media that may alter the continuous alumina layer or the amounts of free iron on the exterior of the oxide scale available for sulfidation. These samples have not reached the same percentage of mass gain as the others when there was a noticeable decrease in mass gain rate. It is believed that FAS and FAL and samples #2 would mimic the same trend as the others alloys and have a decreasing rate of mass gain after another two-hundred and fifty hours, approximately.

The total mass gain of the filter samples exposed for 24,000 hours (using FAS samples #3), the desired life of the elements, has been projected between 1.6% and 2.4% (**Figure 159** and **Figure 160**) using two extrapolation techniques. Extrapolations assume that there is no drastic change in the corrosion mechanism acting upon the alloys. The extrapolations did not take into account the reduction in overall mass gain of the samples after cleaning. This would lower the projected mass gain, however, it is not possible to know if this mass gain, from soot deposition, was linear or parabolic.

The linear extrapolation done for the projected mass gain, after 24,000 hours of exposure, was done using a best fit of the points forming the plateau (500 - 1,500 hours) after the initial mass gain (**Figure 159**). This would be a crude method to use for a solid material. For a porous material that has demonstrated a marked increase in mass upon the first portion of the exposure, this type of extrapolation can be useful. The linear fit gave a mass gain of 2.4% after 24,000 hours.

A parabolic fit was done on the entire curve that allows a more traditional estimation of the mass gain of the porous alloy. This fit is in close agreement with the final three points of FAS sample #3. This gave a final mass gain of 1.6% after 24,000 hours.

4.3.1.2 *Pressure Drop*

The press drop increase of the samples paralleled the mass gain of the samples (**Figure 161**). The marked increase on the pressure drop of FAL sample #1 was from the plastic spacer. FAS and FAL samples #2 had a lower rate of pressure drop increase. This could be related to slight differences in sintering and preoxidation.

The samples exposed for 500 hours (samples #1) had pressure drop increases of 62% and 76% for the FAS and FAL alloys, respectively. Once they were cleaned, they had increases of 38% for the FAS and 46% for the FAL. The FAL sample had and retained a higher pressure drop from the plastic spacer.

Samples #2 (1000 hours of exposure) had increases of 48% and 39% in pressure drop for the FAS and FAL alloys, respectively. These are much lower than the increase seen from the samples exposed for only five hundred hours. After ultrasonic cleaning, the samples

had an overall increase of 3% for the FAS and 8% for the FAL. Most of the pressure drop increase for these samples was caused by the deposition of soot in the pores.

The FAS and FAL samples exposed for 1,500 hours (samples #3) had a total pressure drop increase of 115%. This is an acceptable pressure drop increase. After the samples were ultrasonically cleaned, they had an overall pressure drop increase of 35%. The soot was constricting some of the pores and increasing the pressure drop. Comparing the cleaned pressure drops of samples #1 and #3, the pressure drop increases beyond five hundred hours was caused mainly by soot deposition.

4.3.1.3 *Bubble Points*

The plots of the first and tenth bubble points do not indicate any trends (Figure 162 and Figure 163). For materials that are not affected by the exposure atmosphere, the bubble points do not offer much insight to the overall effect on the media. The simulated IGCC atmosphere does not affect the iron aluminide media significantly enough for the first and tenth bubble points to be useful.

The open bubble point plot (**Figure 164**) show a general increase indicating a decrease in the average pore size of the samples. This trend seems to approximate the same behavior seen with the mass and pressure drop increases. There may be an initial decrease of the outer pores of the media, due to sulfidation of the free iron (see section 4.3.2.7) that does not increase after the first five hundred hours.

The open bubble points of the FAS and FAL samples #2 were not affected until after seven hundred and fifty hours of the exposure time. This is a different response than the other four samples. It may be caused by slight variations in sample preparation and the formation of the continuous alumina scale.

4.3.1.4 *Visual Inspection*

The as-sintered media was a dark grey color. After preoxidation, the media color is a varied "oil slick" color. This is because of variations in the thickness of the thin oxide film causing different levels of interference. After each exposure cycle, the samples would be covered in a black soot. This soot could be smeared but remained on the filter after bubble pointing in Filmex. FAL sample #1 had a black charred section where the plastic had been during the testing. This effectively blinded the media in this area.

4.3.2 Destructive Tests

The destructive test results are presented in **Table 11.**

4.3.2.1 *Carbon/Sulfur*

The carbon content of all the iron aluminide samples did not exceed the typical carbon range. The porous iron aluminide is produced with carbon between 0.08% and 0.17%. There is no indication of carburization. The change in the carbon content of the samples is plotted as **Figure 165.** Carbonization and metal dusting in a hydrogen sulfide containing environment is not thermodynamically possible [10].

All of the samples had an increase in sulfur content (**Figure 166**). This increase is due to the formation of iron sulfides on the upstream surface of the porous media (see section 4.3.2.7). The FAS samples had a lower sulfur increase than the FAL samples. Some reasons for the differences are proposed in section 4.2.7. FAS and FAL samples #2 had a minor percentage increase in sulfur when compared to the other test specimens. This is from the samples having an initially higher sulfur content than the other specimens.

4.3.2.2 *Oxygen/Nitrogen*

There was no significant change in the nitrogen content of the iron aluminide. This is expected because of the lack of nitrogen in the simulated atmosphere.

The oxygen content of the alloys increases upon preoxidation. This is the desired effect of the heat treatment. The oxygen content of the alloys continues to increase during the exposure testing. The alumina scale continues to slowly grow, even in the reducing conditions. Extremely low partial pressures of oxygen are needed for the alumina scale to grow.

4.3.2.3 *Ring Burst Strength Test*

The strength of the FAS media was not affected by the exposure in the simulated IGCC conditions. There was a measured decrease in strength of approximately 8% (Figure 167). This decrease is within the error of the ring burst test. Strength loss of the media does not seem to be a limiting factor in FAS element's life expectancy.

The FAL sample had a marked decrease in strength after five hundred hours of exposure (**Figure 167**). The rate of decrease remained constant, within the error of the burst test, for the entire exposure test. This indicates that the decrease in strength occurs in the first five hundred hours and does not measurably continue. The reason for the decrease in strength of the FAL and not the FAS is not currently known. It is not possible to project the failure of the FAL media based on this data.

4.3.2.4 *Ductility (Ring Crush Test)*

Both of the iron aluminide alloys retained some ductility throughout the exposure testing. After 1,500 hours of testing the samples had a change of ductility of 10% and -17% for the FAS and FAL samples, respectively. These are minor changes considering the low ductility of the iron aluminide alloys. There were no clear trends on the behavior of the ductility of the iron aluminide samples. However, it should be noted that the ductility measurements are qualitative and the comparisons have been made with caution.

4.3.2.5 *Pore Distribution*

The graphs of the pore distributions (**Figure 168 - Figure 177**) show that there are no major changes in the average pore size of the media during the exposure testing. The pore size is decreased slightly during the preoxidation of the alloys. The growth of the alumina scale slightly reduces the pores of the iron aluminide media. The changes seen on the plots of the pore distribution are difficult to quantify and comparisons can have errors.

The pore distributions for the FAS media show that the pore size decreases slightly with time. This is probably from the formation of the iron sulfides on the upstream surface of the samples (see section 4.3.2.7). The FAL media's pore distribution shows increasing pore size with time.

4.3.2.6 *Surface Area*

The preoxidized control samples had surface areas of 0.05 and 0.04 m^2/g for the FAS and FAL samples, respectively. The FAS samples had a decrease in surface area for the first one thousand hours of exposure. After 1,500 hours, the FAS samples had returned to the 0.05 m^2/g. It is unclear why there was a decrease in surface area.

The FAL samples experienced an increase in surface area over the entire exposure testing. After 1,500 hours of the exposure the FAL sample had a surface area of 0.09 m^2/g. The increase in surface area is probably due to the formation of crystals on the upstream surface of the media.

4.3.2.7 *Scanning Electron Microscope Examination*

All of the SEM images are contained in Appendix VII. The images are sub-divided into alloy type and exposure time within the appendix.

4.3.2.7.1 Control samples

The control images for the FAS and FAL samples (Figure 178 - Figure 187 and Figure 219 - Figure 227) are typical for preoxidized iron aluminide samples. The dark inclusions seen on the cross-sections are alumina. Light inclusions have been determined to be mainly zirconium. Both types of inclusions are from the water atomization of the alloy.

The upstream surfaces of the controls are covered with small light nodules composed mainly of zirconium. It is presumed that these are actually zirconia. Previous qualification of the iron aluminide powder has not found zirconium, in significant amounts, on the particle surface. The zirconium is diffusing to the surface of the metal particles during sintering. There are occasionally some darker spots on the surface of the particles. These are mainly composed of alumina. None of these sites were documented during this investigation.

The fracture surfaces of the control samples show some of the broken sinter bonds. These are clean transgranular brittle fractures. Most of the fractures occur at the sinter bonds. There appears to be some porosity in the bonds. The FAL alloy has a higher level of porosity in the sinter bonds. The increased amount of porosity in the sinter bonds of the FAL samples probably has a strong influence on the inferior mechanical properties compared to the FAS.

4.3.2.7.2 Samples exposed for 500 hours.

The cross-sections of the FAS and FAL media (**Figure 188 - Figure 191** and **Figure 228 - Figure 231**) show a layer of crystals on the upstream surface of the media. This layer does not continue into the depth of the media. A partial field spectrum of the layer reveals that it is composed primarily of iron and sulfur. These crystals are believed to be iron sulfides. The base metal has not been affected. A thin alumina layer formed during preoxidation separates the layer of iron sulfides and the base metal. This acts as a diffusion barrier preventing the rapid transport of either sulfur into the base metal or iron out.

The iron sulfides form from free iron on the surface. The free iron was available on the outer surface of the alumina scale because of transient oxidation [11]. This occurs during the preoxidation step when the mixture of iron, chromium and aluminum oxides formed from initial adsorption are separated from the base metal by a continuous film of alumina. The alumina layer then thickens to become a protective oxide. The current method of preoxidation forms a gamma-alumina, based on the 800°C process temperature.

The upstream surface of both alloys was covered in crystals (Figure 192 - Figure 195 and Figure 232 - Figure 234). A full screen spectrum of each alloy had a substantial peak for iron and sulfur, from iron sulfides. The upstream pores were not constricted from the formation of the iron sulfides. The fracture samples were similar to the control samples. Full screen spectra revealed only small amounts of sulfur. No iron sulfide crystals were found.

4.3.2.7.3 Samples exposed for 1000 hours.

The upstream edge of the sample cross-sections for the FAS and FAL were covered with approximately the same amount of iron sulfides as the samples exposed for five-hundred hours (Figure 199 - Figure 202 and Figure 240 - Figure 243). These samples are from a different sintering and preoxidation lot than the others. This could cause differences in the formation of the oxide scale and the amount of iron left on the external surface of the alumina scale. The base metal of both alloys was not affected by the exposure conditions. The upstream surfaces of both alloys (Figure 203 - Figure 205 and Figure 244 - Figure 246) were covered with the same amount of iron sulfide crystals as the samples exposed for five hundred hours.

The fracture samples for both alloys (Figure 206 - Figure 208 and Figure 247 - Figure 249) did not have any iron sulfide crystals on the metal particle surface. These images were collected towards the center of the media thickness. Both alloys demonstrated the typical clean transgranular brittle fracture that is found on most iron aluminide. The full screen spectrum of both samples was a typical preoxidized iron aluminide spectrum. The oxygen peaks are from the alumina layer formed during preoxidation.

4.3.2.7.4 Samples exposed for 1500 hours.

The cross-sections of the FAS and FAL alloys (Figure 209 - Figure 212 and Figure 250 - Figure 255) were very similar to those of the samples exposed for five-hundred hours. There were not any significant increase in the formation of iron sulfides on the upstream surface of the media. There were no indications of attack of the base metal or grain boundaries. The partial field spectra of the base metal close to the upstream surface did not contain any sulfur.

The upstream surfaces of the samples (Figure 213 - Figure 215 and Figure 256 - Figure 258) were covered in iron sulfide crystals. These have the same morphology as those seen on the samples exposed for five hundred hours. The upstream surface maintains open pores that are not significantly obstructed by the formation of the sulfides.

The fracture samples for both alloys (Figure 216 - Figure 218 and Figure 259 - Figure 261) were similar to the control images. The fracture surfaces had some porosity and were clean and transgranular. Full screen spectra revealed no sulfur for the FAS and nearly undetectable sulfur for the FAL.

4.4 Manufacture of Fifty Filters

4.4.1 Quality Control Procedures

4.4.1.1 *Traceability of Raw Materials*

4.4.1.1.1 Iron Aluminide Powder

Metal powders were purchased in accordance with the specifications listed in Pall Engineering Procedure MMP EP-004. This is a Pall Trinity Micro (PTM) Industrial Process (IP) internal manufacturing procedure that lists the requirements for powder properties such as particle size distribution, chemical composition, and density. All metal powders purchased by Pall are manufactured and identified by lot number. The powder vendor is required to supply a test report for each powder lot.

4.4.1.1.2 Hardware Materials

Upon request, Pall can supply material certification documentation pertaining to the product form and composition of hardware used in the manufacture of porous metal filter elements. Where required by the customer, material certification must be requested in writing at the time that the filter elements are ordered.

4.4.1.2 *Product Inspection Methods*

Iron aluminide filter element assemblies receive quality assurance verification by Pall Manufacturing Procedure MP-P009. This specifies the procedures for final inspection and testing of metal element assemblies including visual, dimensional, filter performance, and welded joint requirements.

4.4.1.3 *Processing Instructions*

Filter media is produced according to the requirements listed in Pall Manufacturing Procedure IP MP-17. This is a PTM internal manufacturing control procedure that regulates all the filter media production processes. Areas controlled by IP MP-17 include preparation of raw materials, fabrication of seamless media tubes, media sintering, and qualification of finished cylinders.

4.4.1.3.1 Raw Materials

IP MP-17 includes documentation procedures for the powder lots used and requirements that specify the types and quantities of materials required for preparing the powder mixture.

4.4.1.3.2 Fabrication of Seamless Cylinders

IP MP-17 includes specifications for the processing equipment required for unit cylinder formation, documentation requirements, and detailed instructions for all phases of the seamless cylinder formation process.

4.4.1.3.3 Sintering of Media Cylinders

IP MP-17 includes specifications for process documentation, as well as detailed processing requirements such as sintering temperatures, times and atmospheres. Also included are specifications for furnace load size and cylinder arrangement.

4.4.1.3.4 Qualification Testing of Sintered Medium

MMD MP-17 includes qualification requirements for batches of sintered filter media. Furnace batches are qualified by performing a random sampling on three or more tubes selected from each sinter load. The sampling includes testing procedures and acceptance criteria for media airflow permeability, bubble point flow, wall thickness, tensile strength, and appearance. Preliminary qualification criteria for S-Series PSS® 2% chromium iron aluminide are included in the attached specification sheet (Appendix VIII).

4.4.1.4 *Bills of Materials*

Material requirements for iron aluminide element assemblies are controlled via the bill of materials system per Pall Engineering Procedure IP EP-011. Bills of materials specify the type and quantity of each component used to manufacture a complete filter assembly.

4.4.1.5 *Control Drawings*

Dimensional requirements for iron aluminide element assemblies are controlled via the drawing control system per Pall Engineering Procedure IP EP-003. Control drawings specify critical dimensional, performance, material, and process specifications required for manufacturing complete filter assemblies.

4.4.2 Quality Assurance Tests

4.4.2.1 *Dimensional Conformance*

The thickness of the as-sintered media is controlled by the amount of powder used for spinning the seamless cylinder and the amount of pressure applied during the consolidation step.

4.4.2.2 *Media Strength*

Media strength is evaluated in terms of ultimate hoop strength. The hoop strength for individual media cylinders is determined using the ring burst test procedure, specified in Pall Engineering Procedure IP EP-29. This procedure determines tensile strength by internally pressurizing a short (1" long) media sample until failure. The ultimate hoop strength is then calculated using the pressure at the time of failure and the dimensions of the sample ring.

4.4.2.3 *Filter Properties*

4.4.2.3.1 Permeability

Permeability is a measurement of the airflow pressure drop while passing a given volume of air through a given area of media. The test is conducted by flowing air from the inside of the media and measuring the pressure drop and volumetric flow. The measured values with the total media area are used to calculate permeability (psi/acfm/ft^2). The element must fall within a predetermined ranged to be acceptable.

4.4.2.3.2 Removal Efficiency

The media's removal efficiency was determined using a modified F2 test method. Testing was conducted on filters from several different production runs to measure the media's removal efficiency by weight for particles of a given size and larger. This results in the equivalent gas removal efficiency. The removal efficiency test is performed in accordance with Pall Scientific Laboratory Service (SLS) Test Procedure F2-01.

4.4.2.3.3 Blowback Performance

The media's blowback recovery performance was evaluated by the Pall Process Equipment Development (PED) Department's Filter Performance Laboratory in accordance with the parameters specified in PED document #17-011; Procedure BBT-25. The test involves challenging the media with contaminant of controlled particle distribution under fixed conditions of forward face velocity, particulate ingression rate, and reverse pulse (blowback) gas face velocities. The media's recovery permeability (the permeability immediately after reverse cleaning) is recorded for each forward/reverse cycle. Testing continue until the media's recovery permeability is stable (that is, within certain guidelines, the recovery permeability remains constant over a given number of cycles).

4.4.2.3.4 First Bubble Test

The first bubble test is used to assure that the filter's largest pore does not exceed a predetermined maximum size. The test is conducted by submerging the filter in a specific wetting fluid (Filmex-B). Then gradually increasing the air pressure inside the filter until the first bubble stream appears. The first bubble point pressure must meet or exceed a specified minimum value.

4.4.2.3.5 Open Bubble Test

The open bubble test roughly determines the filter's average pore size. It is conducted by submerging the filter in a wetting fluid (Filmex-B). The filter's internal air pressure is adjusted to meet a predetermined volumetric flow. The air pressure is checked to verify that it falls within the acceptance range.

4.4.3 Production of Fifty Filters

Task 5 required the manufacture and qualification for shipment of fifty iron aluminide filter elements. The fifty elements were designated by the United States Department of Energy for installation and operation at two testing sites; The Sierra Pacific Power / Pinon Pine facility in Sparks, Nevada; and the Dynegy Power Corporation plant in Terre Haute, Indiana. A total of forty-six 1.5 meter long elements were manufactured for the Dynegy Power Corporation facility; an IGCC gasifier which typically operates at around 700 degrees F. The remaining four filter elements (also 1.5 meters in length), were built for the IGCC gasifier operated by Pinon Pine. Some control samples have been retained for comparison with future post-exposure evaluations.

The fifty filter elements were manufactured in accordance with Pall Manufacturing Procedure W5X, and the Pall PTM process sheet control procedure IP EP-005. W5X specifies requirements for metal element fabrication including component handling, weld preparation, welding processes, and post weld inspection. IP EP-005 lists the requirements for product specific process sheets, thus providing a means for relaying job-specific processing instructions on individual customer orders.

5.0 CONCLUSIONS

The FAS alloy has an extrapolated mass gain between 1.6 and 2.4 wt% after 24,000 hours (2.7 years) of exposure. This is an acceptable mass increase. It is believed that the media can operate beyond 24,000 hours.

Iron aluminide porous metal media is now commercially available. The FAS alloy has been successfully moved into manufacturing.

The FAS and FAL alloys are both corrosion resistant in IGCC atmospheres. Both of the alloys preformed similarly over various exposure conditions. The FAS alloy is favored for use in most conditions because it did not have a reduction in strength in the long-term exposure testing.

6.0 RECOMMENDATIONS

Post-exposure evaluation of the elements manufactured for Pinon Pine and Dynegy should be conducted jointly between Oak Ridge National Laboratory and Pall Process Equipment Development.

Iron aluminide hot gas filters should be tested in available IGCC's and PFBC's. Laboratory testing of the media has been successful. The media now needs to be exposed to actual conditions containing ash and char.

The iron aluminide media allows increasing temperatures to 1200°F in IGCC's. Higher temperatures may be possible but are untested in reducing sulfur-bearing environments.

7.0 REFERENCES

[1] Tortorelli, P.F. and De Van, J.H., Compositional Influences on the High Temperature Corrosion Resistance of Iron Aluminides, Article in Processing, Properties, and Applications of Iron Aluminides, ED. J.H. Schneibel and M. A. Crimp, 1994, p 261.

[2] Data Package on Fe_3Al-FeAl Based alloys Developed at ORNL, Compiled by Vinod K. Sikka, January 20, 1993.

[3] Tortorelli, P.F. and DeVan, J.H., Behavior of Iron Aluminides in Oxidizing / Sulfidizing Environments, Materials Science and Engineering, A153 (1992), 573-577.

[4] De Van, J.H. and Tortorelli, P. F., The Oxidation - Sulfidation Behavior of Iron Alloys Containing 16-40 AT% Aluminum, Corrosion Science, Vol. 35,Nos 4-8, pp1065-1071,1993.

[5] De Van, J.H., Oxidation Behavior of Fe3Al and Derivative Alloys, Oxidation of High Temperature Intermetallics Ed. by T. Grobstein and J. Doychak, The Minerals, Metals & Materials Society, 1989.

[6] De Van, J.H. Corrosion Performance of Iron Aluminide (Fe3Al) in Coal Conversion Process Environments, Heat Resistant Materials, Proceedings of the First International Conference, Fontana Wisconsin, September 23-26,1991.

[7] De Van, J.H., "Development of Surface Treatments and Alloy Modifications for Corrosion Resistant Oxide Scales." Article in Proceedings of the Fourth Annual Conference on Fossil Energy Materials, compiled by R.R. Judkins and D.N. Braski, August 1990, pps 299-309.

[8] International Organization of Standards. International Standard 4003, Permeable sintered metal materials - Determination of bubble test pore size. 1977

[9] Per Kofstad, *High Temperature Corrosion*, Elsevier Applied Science, New York, p156

[10] J. H. DeVan, P. F. Tortorelli, R. R. Judkins, and I. G. Wright, "Carbon Formation and Metal Dusting in Advanced Coal Gasifiaction Processes", ORNL/TM-13014, Oak Ridge National Lab, February 1997

[11] G. C. Wood and F. H. Scott, "Oxidation of alloys", Materials Science and Technology, Vol.3 July 1987

APPENDIX I: DRAWINGS

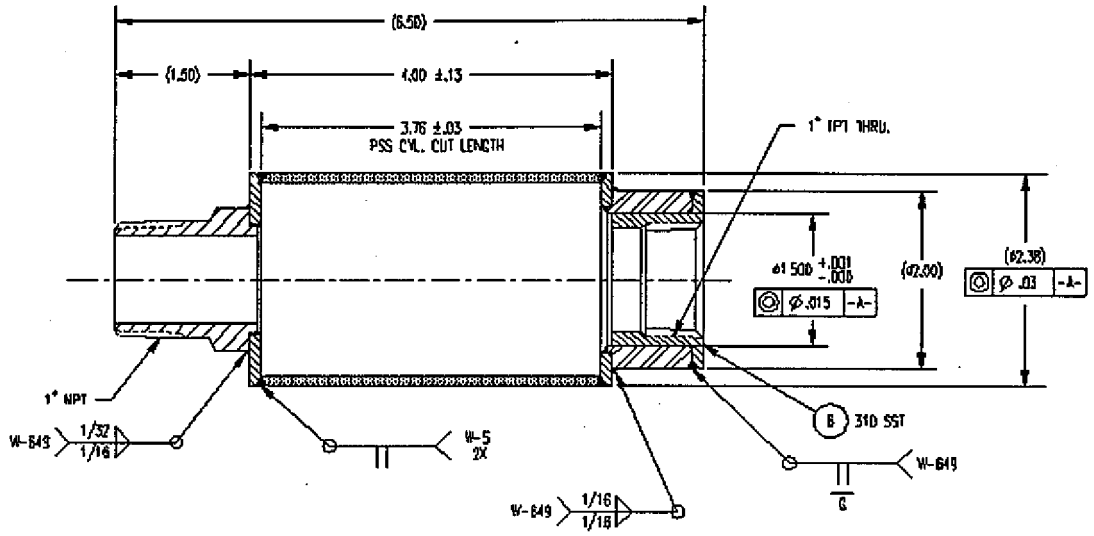

Figure 1: Filter for short-term testing.

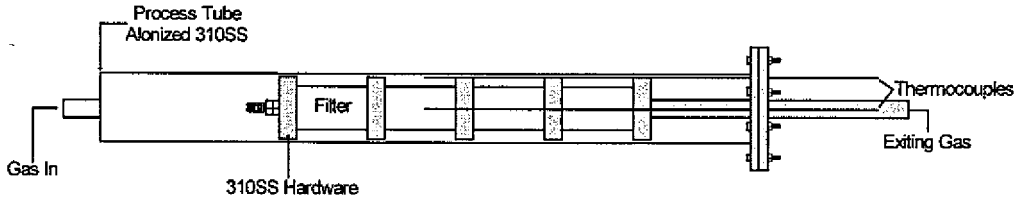

Figure 2: Schematic of process tube and test jig for long term exposure.

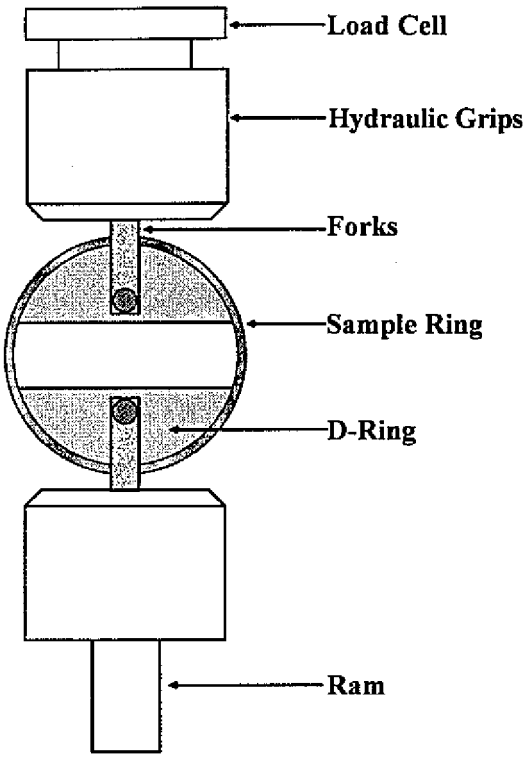

Figure 3: Schematic of D-ring Tensile test.

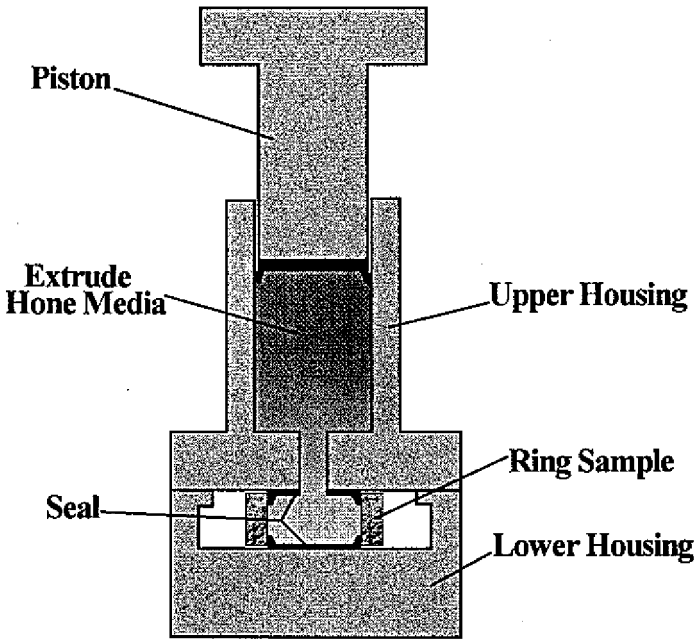

Figure 4: Schematic of the ring burst test.

APPENDIX II: TABLES

Table 1: Representative IGCC Atmospheres and Simulated Atmosphere for Exposure Testing

Types of Atmosphere	Oxygen Blown Tampa Electric	Air Blown Sierra Pacific	Simulated* Atmosphere (w/o Nitrogen) w/ chlorides
Temperature °F	900 - 925	1000 - 1050	925
Pressure	400 psia 26.1 atm	272 - 275 psia	~ 1 atm
Component	Mole %	Mole %	Mole %
CO	40.36	28.89	37
H_2	28.20	14.57	34
CO_2	10.34	5.44	17
H_2O	14.16	5.50	10
CH_4	0.15	--	1.0
Ar	0.94	0.60	--
N_2	5.13	48.65	--
COS	0.02	--	--
O_2	0.00	0.00	0.00
H_2S	0.63**	0.03**	Variable
HCl	NA	NA	80 ppm
NaCl	NA	NA	2x*** 2 ppm
KCl	NA	NA	2x*** 5.5 ppm

* Corresponds with oxygen blown Tampa Electric, Equilibrated at 1300°F, at 1 bar with no nitrogen.

** Upstream of final desulfurization which is expected to lower H_2S to 0.003% (30 ppm)

*** Amount added

Note: Temperatures and pressures supplied by FETC (Morgantown).

Table 2: Exposure Conditions for Short-term Exposure Testing

Temperature	925°F		1050°F	1200°F
Gasifier	Tampa Electric		Sierra Pacific	
Variable (s)				
H_2S %		0.0783	0.0783	
Temp. °F		925	1050	
Pulse		N	Y	
Chlorides		N	Y	
Run #		1	5	
Variable (s)				
H_2S %	0.783			0.783
Temp. °F	925			1200
Pulse	Y			Y
Chlorides	Y			Y
Run #	4			2
Variable (s)				
H_2S %	7.83			7.83
Temp. °F	925			925
Pulse	Y			Y
Chlorides	Y			Y
Run #	3			6

Comparison of Test Atmosphere and Actual Atmosphere*

H_2S Level Used for Short-term Exposure Test with Simulated Atmosphere at 1 atmosphere	Equivalent H_2S Level in Oxygen Blown Gasifier at 26.1 atmospheres
0.0783 vol%	0.007 mol%
0.783 vol%	0.072 mol%
7.83 vol%	0.72 mol%

* Calculated by Peter Tortorelli of Oak Ridge National Laboratory.

Table 3: Powder Chemical Composition as Reported by Vendor

Alloy	C	Al	Fe	Cr	Zr	B	O
FAS	0.038	17.11	Bal	2.19	0.17	--	0.50
FAL	0.046	15.75	Bal	5.49	0.17	--	0.38
FAS-0% Cr	0.024	22.78	Bal	--	0.16	0.008	0.73

* Carbon (wt %) contents of the powders were higher than expected.
* Oxygen increased, as expected, with increasing aluminum content.
* All three compositions were melted as 500 pound air induction melts, water atomized and sieved to a -100 + 325 mesh.

Table 4: Physical Powder Properties

	FAS	FAL	FAS-0% Cr
Mesh Size[a]	(wt.%)	(wt.%)	(wt.%)
+100	5.0	5.1	6.1
+120	5.0	5.4	6.3
+140	10.1	10.5	11.5
+200	30.3	30.1	30.3
+270	25.6	26.2	27.3
+325	18.3	13.7	14.3
-325	5.7	9.0	4.2
Apparent Density[a] (g/cc)	1.73	1.74	1.62
Flow Time[a] Sec. For 50g	50	49	53
Surface Areas			
Single point area	0.34	0.22	0.52
Multipoint area (m^2/g)	0.35 ± 0.04[b]	0.22 ± 0.02[b]	0.53 ± 0.05[b]

* Size distributions were similar for compositions FAS, FAL and FAS-0% Cr.
* Flow times were similar.

[a] Engineering Procedure #IP EP-4 Rev. H

[b] Estimated error based on 2x standard deviation of multiple determinations of CRM M11-06, an alpha alumina with a reported surface area of 0.23 m^2/g.

Table 5: Summary of Mechanical and Filter Properties versus Sintering Temperature

	Sintering Temperature (°F)	FAS	FAL	FAS-0% Cr
Ductility (%)	2310	5.9	4.9	3.2
	2345	7.3	5.7	5.2
	2385	6.9	5.9	6.6
	2420	8.0[a]	(b)	6.4
Ring Burst Strength (ksi)	2310	6.4	(b)	(b)
	2345	(b)	5.8	4.8
	2385	11.7	9.9	(b)
	2420	11.9[a]	7.8[a]	2.8
D-Ring Tensile (ksi)	2310	5.7	1.5	1.8
	2345	8.8	5.9	3.5
	2385	4.8	2.2	2.2
	2420	5.9	2.5	4.9
Pressure Drop (in. H_2O)	2300	23.2	23.0	15.9
	2310	27.6	(b)	(b)
	2345	23.7	(b)	(b)
	2420	20.2	19.9	36.2
Open Bubble Point (in. H_2O)	2300	29.0	33.2	26.8
	2310	30.1	(b)	(b)
	2345	28.8	(b)	(b)
	2420	28.6	28.7	32.2

a: The binder content of these samples was half the standard amount
b: No results are available

Table 6: Data for Chemical and Mechanical Properties for As-Sintered FAS

Carbon (wt%)

Sintering Temperature (°F)	2300	2310	2345	2385	2420
Number of Samples	1	6	1	2	34
Concentration of Carbopol	1	1	1	1	½
Mean	0.1613	0.1745	0.1793	0.14805	0.1240
Standard Deviation		0.0170		0.00007	0.0183
Maximum		0.2074		0.1481	0.1656
Minimum		0.1619		0.1480	0.0856

Sulfur (wt%)

Sintering Temperature (°F)	2300	2310	2345	2385	2420
Number of Samples	1	6	1	2	34
Concentration of Carbopol	1	1	1	1	½
Mean	0.0143	0.01075	0.0182	0.0179	0.00839
Standard Deviation		0.00182		0.00481	0.00466
Maximum		0.0138		0.0213	0.0176
Minimum		0.0082		0.0145	0.0005

Chromium (wt%)

Sintering Temperature (°F)	2300	2310	2345	2385	2420
Number of Samples	1	(1)	1	(1)	32
Concentration of Carbopol	1		1		½
Mean	2.42		2.01		2.132
Standard Deviation					0.1523
Maximum					2.69
Minimum					1.88

Ring Burst Strength (psi)

Sintering Temperature (°F)	2300	2310	2345	2385	2420
Number of Samples	(1)	1	(1)	1	3
Concentration of Carbopol		1		1	½
Mean		6391		11707	11893
Standard Deviation					2356
Maximum					13639
Minimum					9213

D-ring Tensile (psi)

Sintering Temperature (°F)	2300	2310	2345	2385	2420
Number of Samples	1	8	1	2	10
Concentration of Carbopol	1	1	1	1	½
Mean	5944	5754	8813	4845	5882
Standard Deviation		3841		1443.2	2483.6
Maximum		12880		5866	9910
Minimum		2314		3825	2713

Ductility (%)

Sintering Temperature (°F)	2300	2310	2345	2385	2420
Number of Samples	1	8	1	2	11
Concentration of Carbopol	1	1	1	1	½
Mean	5.6	5.85	7.3	7.1	8.097
Standard Deviation		1.1058		1.414	1.1923
Maximum		7.9		8.1	9.72
Minimum		4		6.1	5.99

(1) No Data Available

Table 7: Data for Chemical and Mechanical Properties for As-Sintered FAL

Carbon (wt%)					
Sintering Temperature (°F)	**2300**	**2310**	**2345**	**2385**	**2420**
Number of Samples	1	(1)	2	1	2
Concentration of Carbopol	1		1	1	1
Mean	0.1808		0.1879	0.1699	0.2282
Standard Deviation			0.0188		0.0683
Maximum			0.2012		0.2765
Minimum			0.1746		0.1799

Sulfur (wt%)					
Sintering Temperature (°F)	**2300**	**2310**	**2345**	**2385**	**2420**
Number of Samples	1	(1)	2	1	2
Concentration of Carbopol	1		1	1	1
Mean	0.0097		0.0084	0.0093	0.0046
Standard Deviation			0.00056		0.00339
Maximum			0.0088		0.007
Minimum			0.0080		0.0022

Chromium (wt%)					
Sintering Temperature (°F)	**2300**	**2310**	**2345**	**2385**	**2420**
Number of Samples	1	(1)	(1)	1	2
Concentration of Carbopol	1			1	1
Mean	5.28			4.97	4.73
Standard Deviation					0.523
Maximum					5.1
Minimum					4.36

Ring Burst Strength (psi)					
Sintering Temperature (°F)	**2300**	**2310**	**2345**	**2385**	**2420**
Number of Samples	(1)	(1)	1	1	1
Concentration of Carbopol			1	1	1
Mean			5816	9933	7733
Standard Deviation					
Maximum					
Minimum					

D-ring Tensile (psi)					
Sintering Temperature (°F)	**2300**	**2310**	**2345**	**2385**	**2420**
Number of Samples	1	1	2	1	1
Concentration of Carbopol	1	1	1	1	1
Mean	5333	1472	5947	2182	2505
Standard Deviation			868.3		
Maximum			6561		
Minimum			5333		

Ductility (%)					
Sintering Temperature (°F)	**2300**	**2310**	**2345**	**2385**	**2420**
Number of Samples	1	1	2	1	(1)
Concentration of Carbopol	1	1	1	1	
Mean	5.8	4.9	5.7	5.9	
Standard Deviation			0.141		
Maximum			5.8		
Minimum			5.6		

(1) No Data Available

Table 8: Data for Chemical and Mechanical Properties for As-Sintered FAS-0% Cr

Carbon (wt%)					
Sintering Temperature (°F)	2300	2310	2345	2385	2420
Number of Samples	1	(1)	1	1	2
Concentration of Carbopol	1		1	1	1
Mean	0.1628		0.1929	0.1332	0.1522
Standard Deviation					0.0401
Maximum					0.1806
Minimum					0.1238
Sulfur (wt%)					
Sintering Temperature (°F)	2300	2310	2345	2385	2420
Number of Samples	1	(1)	1	1	2
Concentration of Carbopol	1		1	1	1
Mean	0.0050		0.0023	0.0014	0.0042
Standard Deviation					0.00254
Maximum					0.006
Minimum					0.0024
Chromium (wt%)					
Sintering Temperature (°F)	2300	2310	2345	2385	2420
Number of Samples	1	(1)	(1)	(1)	1
Concentration of Carbopol	1				1
Mean	0.257				0.16
Standard Deviation					
Maximum					
Minimum					
Ring Burst Strength (psi)					
Sintering Temperature (°F)	2300	2310	2345	2385	2420
Number of Samples	(1)	(1)	1	(1)	1
Concentration of Carbopol			1		1
Mean			4800		2809
Standard Deviation					
Maximum					
Minimum					
D-ring Tensile (psi)					
Sintering Temperature (°F)	2300	2310	2345	2385	2420
Number of Samples	1	1	1	1	4
Concentration of Carbopol	1	1	1	1	1
Mean	2680	1848	3510	2178	4881.4
Standard Deviation					1835.5
Maximum					7538
Minimum					3592
Ductility (%)					
Sintering Temperature (°F)	2300	2310	2345	2385	2420
Number of Samples	1	1	1	1	1
Concentration of Carbopol	1	1	1	1	1
Mean	6.4	3.2	5.2	6.6	6.4
Standard Deviation					
Maximum					
Minimum					

(1) No Data Available

Table 9: Chemical and Mechanical Properties of Short-Term Exposures

Filter ID	Cr (wt%)	Pre-oxidation	Exposure	Temperature (F)	H2S (vol%)	Chlorides (Y/N)	Void Volume (%)	Carbon (wt%)	Sulfur (wt%)	Chromium (wt%)	Oxygen (ppm)	Nitrogen (ppm)	Ductility (%)	Tensile (psi)	Putty Ring BurstTest Break Load (lbs)	Putty Ring BurstTest MOR (psi)
T-29	2	--	Unexposed				49.58	0.1780	0.0215	2.01	2245	28	7.3	8813.0	(a)	(a)
T-29-2	2	800°C	Run 1	925	0.0783	N	---	0.1748	0.0506	---	3056	<10	4.6	5407.0	1104.28	6090
T-29-7	2	--	Run 1	925	0.0783	N	---	0.1773	0.0523	---	1160	1	3.2	3918.0	1370.70	6574
T-29-8	2	800°C	Run 2	1200	0.783	Y	---	0.1672	0.0897	---	8290	<10	6.4	5305.5	2890.93	15744
T-29-9	2	--	Run 2	1200	0.783	Y	---	0.1865	0.1313	---	7700	<10	5.8	7145.0	2312.93	10114
T-42	2	--	Unexposed				45.59	0.1678	0.0163	2.42	1860	10	5.6	5944.0	(a)	(a)
T-42-2	2	--	Run 3	925	7.83	Y	---	0.1808	0.0564	---	732	<10	5.3	4375.5	2142.10	9838
T-42-7	2	800°C	Run 3	925	7.83	Y	---	0.1499	0.0530	---	7865	<10	4.2	6282.5	1902.62	8477
T-42-8	2	800°C	Run 4	925	0.783	Y	---	0.1474	0.0536	2.08	3779	13	--	6710.0	350.05	1588
T-42-9	2	800°C	Run 4	925	0.783	Y	---	0.1660	0.0467	2.25	1299	<10	--	4741.5	2364.35	10820
T-77-C	2	800°C	Unexposed				53.45	0.0903	0.0107	2.34	1633	<10	7.1	6802.0	3130.04	12571
T-77-C1	2	800°C	Run 5	1050	0.0783	Y	---	(a)	(a)	---	2835	<10	5.5	6126.0	1204.53	6272
T-78-C	2	--	Unexposed				50.83	0.1105	0.0168	2.25	1326	<10	9.6	6758.0	2795.41	12102
T-78-C1	2	--	Run 5	1050	0.0783	Y	---	(a)	(a)	---	3115	<10	5.8	7146.5	1041.72	5391
T-173-Con-1	2	--	Unexposed				41.00	0.1215	0.0094	2.55	--	--	5.6	--	1944.58	9574
T-173-Con-2	2	800°C	Unexposed				43.00			--	--	--	6.3	--	3198.64	16929
T-173-Con-3	2	1000°C	Unexposed				42.00			--	--	--	5.4	--	4068.91	19139
T-173-C-1	2	800°C	Run 6	1200	7.83	Y	--	0.0973	0.0805	--	--	--	6.5	--	2356.87	12460
T-173-C-2	2	1000°C	Run 6	1200	7.83	Y	---	0.1488	1.5350	--	--	--	(a)	--	(a)	(a)
T-43	0	N	Unexposed				49.20	0.1628	0.0050	0.257			6.4	2680.0	(a)	(a)
T-43-2	0	800°C	Run 1	925	0.0783	N	---	0.1337	0.2864	---	8095	8	5.3	3159.0	886.38	3116
T-43-9	0	800°C	Run 2	1200	0.783	Y	---	0.1247	0.4567	---	10900	<10	3.4	2681.5	751.50	4200
T-43-8	0	800°C	Run 3	925	7.83	Y	---	0.1061	0.3313	---	3209	<10	5.4	4250.5	904.54	6253
T-55-A	0	800°C	Unexposed				58.67	0.1439	0.0037	0.22	5485	54	2.9	3259.0	804.90	2540
T-55-A1	0	800°C	Run 5	1050	0.0783	Y	---			---	14200	72	2.7	756.0	(b)	(b)
T-40	5	--	Unexposed				43.29	0.1808	0.0097	5.28	1125	58	5.8	5333.0	(a)	(a)
T-40-2	5	800°C	Run 1	925	0.0783	N	---	0.1780	0.0324	---	1645	<10	3.6	5269.0	747.07	3511
T-40-8	5	800°C	Run 2	1200	0.783	Y	---	0.1664	0.0368	---	2161	<10	9.7	4701.5	1232.15	6125
T-40-9	5	800°C	Run 3	925	7.83	Y	---	0.1716	0.0473	---	991	<10	3.4	4532.0	1875.61	9181
T-36	5	--	Unexposed				46.65	0.1699	0.0093	4.97			5.9	2182.0	1985.02	9933
T-36-8	5	800°C	Run 4	925	0.783	Y	---	0.1648	0.0374	5.52	3580	<10		3901.5	1513.67	7653
T-92-B	5	800°C	Unexposed				53.64	0.1566	0.0028	5.15	2871	31	6.8	4428.0	2132.00	10147
T-92-B1	5	800°C	Run 5	1050	0.0783	Y	---	(a)	(a)	---	6870	40	4.3	4376.0	(b)	(b)
T-146-BB-Con-1	5	--	Unexposed				42.00	0.1108	0.0100	5.58	--	--	8.2	--	1123.66	6100
T-146-BB-Con-2	5	800°C	Unexposed				43.00			--	--	--	6.6	--	923.00	5353
T-146-BB-Con-3	5	1000°C	Unexposed				41.00			--	--	--	5.8	--	1396.64	7633
T-146-BB-1	5	800°C	Run 6	1200	7.83	Y	--	0.1021	0.0789	--	--	--	(a)	--	349.66	1848
T-146-BB-2	5	1000°C	Run 6	1200	7.83	Y	--	0.0941	0.9494	--	--	--	5.5	--	719.40	3605

(a) No Data Available
(b) Samples did not fit piston cups (no results available)

Table 11: Chemical and Mechanical Data for Long-Term Exposure Test

Sample ID	Filter ID	Exposure (hours)	Carbon (wt%)	Sulfur (wt%)	Oxygen (wt%)	Nitrogen (wt%)	Ductility (%)	Burst Test MOR (ksi)	Surface Area (m^2/g)
	T-260-C-Con	0	0.126	0.009	0.170	0.006	6.1	12.8	0.05
	IA-66-C-Con	0	0.113	0.049	0.260	0.004	5.6	12.6	0.05
FAS #1	T-260-C-1	500	0.120	0.067	0.210	0.002	4.4	13.0	0.04
FAS #2	IA-66-C	1000	0.108	0.074	0.850	0.004	5.9	11.0	0.03
FAS #3	T-260-C-2	1500	0.105	0.139	0.620	0.012	6.7	11.9	0.05
	T-261-B-Con	0	0.156	0.006	0.530	0.005	4.7	11.4	0.04
	IA-75-B-Con	0	0.123	0.066	0.710	0.004	4.4	14.7	0.04
FAL #1	T-261-B-1	500	0.150	0.105	0.600	0.002	5.3	6.9	0.05
FAL #2	IA-75-B	1000	0.110	0.109	0.590	0.004	4.5	6.4	0.06
FAL #3	T-261-B-2	1500	0.140	0.156	0.600	0.005	3.9	6.1	0.09

APPENDIX III: CALCULATIONS OF SIMULATED ATMOSPHERE

Equilibrium Gas Compositions for Representative IGCC Gasifiers

Table 11 and Table 12 show equilibrium gas compositions that have been calculated for representative oxygen blown and air blown gasifiers. These calculations† were done under the direction of Peter Tortorelli and Jack DeVan (retired) from Oak Ridge National Laboratory.

The equilibrium calculations have been worked out for various temperatures at system pressures and at one atmosphere.

The nitrogen/argon were removed from the mixtures and one atmosphere calculations were redone to try and match the oxygen partial pressure to what it would be at the high pressure. In each case it reduced the discrepancy but did not eliminate it.

The oxygen partial pressures are probably close enough and are conservative in that they are lower than in actual practice.

By eliminating nitrogen in this way the gas compositions are almost equivalent for the oxygen blown and for the air blown cases: a single test gas at one atmosphere can be used to simulate both gasifier environments for the anticipated exposure.

It was pointed out that sluggish kinetics can essentially "freeze in" a gas composition representative of equilibrium at higher temperature. Consequently, the gas composition calculated at 1300°F was chosen even though exposures were to be conducted at lower temperatures. The equilibrium calculations indicate carbon deposition as the temperature falls. However H_2S presence in the exposure environments should inhibit carbon deposition.

† "SOLGASMIX-PV, A COMPUTER PROGRAM TO CALCULATE EQUILIBRIUM RELATIONSHIPS IN COMPLEX CHEMICAL SYSTEMS" by Theodore M. Besman, Published by Oak Ridge National Laboratory, April 1977.

Table 11:Equilibrium Gas Compositions for Oxygen Blown Gasifier (Tampa Electric)

Product Gas (moles) - %	
CO	44.36
CO_2	10.34
H_2	28.20
H_2O	14.16
N_2/Ar	6.07
O_2	0.00
H_2S*	0.63
CH_4	0.15

Temperature: 900 - 925°F**
Pressure: 400 psia, 26.1 atmospheres**

Equilibrated at 1300°F

	Comp. (Bar)		
	At 26.1 bar	At 1 bar	At 1 bar, no N_2
CO	2.95	0.34	0.37
CO_2	8.11	0.16	0.17
CH_4	1.97	8.7×10^{-3}	1.0×10^{-2}
H_2	4.01	0.32	0.34
H_2O	6.76	9.3×10^{-2}	0.10
N_2	2.09	6.2×10^{-2}	--
O_2	5.6×10^{-21}	1.6×10^{-22}	1.7×10^{-22}
H_2S	0.22	6.4×10^{-3}	6.8×10^{-3}
S_2	9.77×10^{-8}	1.3×10^{-8}	1.3×10^{-8}

Equilibrated at 1100°F

	Comp. (Bar)		
	At 26.1 bar	At 1 bar	At 1 bar, no N_2
CO	0.82	0.14	015
CO_2	9.26	0.29	0.32
CH_4	2.46	3.5×10^{-2}	3.9×10^{-2}
H_2	2.22	0.26	0.28
H_2O	8.84	0.19	0.21
N_2	2.27	7.4×10^{-2}	--
O_2	1.3×10^{-23}	4.0×10^{-25}	4.4×10^{-25}
H_2S	0.24	7.6×10^{-3}	8.3×10^{-3}
S_2	$2.2\ 10^{-8}$	1.6×10^{-9}	1.7×10^{-9}

Equilibrated at 925°F

	Comp. (Bar)		
	At 26.1 bar	At 1 bar	At 1 bar, no N_2
CO	0.18	3.5×10^{-2}	3.7×10^{-2}
CO_2	9.39	0.35	0.38
CH_4	2.64	6.1×10^{-2}	6.8×10^{-2}
H_2	1.07	0.16	0.17
H_2O	10.21	0.30	0.33
N_2	2.36	8.3×10^{-2}	--
O_2	1.3×10^{-26}	4.8×10^{-28}	5.3×10^{-28}
H_2S	0.24	8.6×10^{-3}	9.5×10^{-3}
S_2	4.4×10^{-9}	2.4×10^{-10}	2.6×10^{-10}

* Upstream of final desulfidation which is expected to be lower H_2S to 30 ppm

Table 12:Equilibrium Gas Compositions for Air Blown Gasifier (Sierra Pacific)

Product Gas (moles) - %	
CO	23.89
CO_2	5.44
H_2	14.57
H_2O	5.50
N_2	48.65
O_2	0.00
H_2S*	0.03
S_2	0.00
Ar	0.60

Temperature: 900 - 925°F**
Pressure: 400 psia, 26.1 atmospheres**

Equilibrated at 1300°F

	Comp. (Bar)		
	At 20.26 bar	At 1 bar	At 1 bar, no N_2
CO	1.68	0.22	0.42
CO_2	2.65	7.6×10^{-2}	0.16
H_2	2.34	0.17	0.33
H_2O	2.26	3.5×10^{-2}	0.08
N_2	11.17	0.49	--
O_2	1.8×10^{-21}	8.6×10^{-23}	1.1×10^{-22}
H_2S	6.9×10^{-3}	3.0×10^{-4}	6.1×10^{-4}
S_2	2.9×10^{-10}	1.1×10^{-10}	1.1×10^{-10}
Ar	0.14	6.1×10^{-3}	1.2×10^{-2}

Equilibrated at 1100°F

	Comp. (Bar)		
	At 20.26 bar	At 1 bar	At 1 bar, no N_2
CO	0.46	0.10	0.15
CO_2	2.97	0.13	0.32
H_2	1.50	0.15	0.29
H_2O	3.37	7.2×10^{-2}	0.22
N_2	11.81	0.54	--
O_2	4.1×10^{-24}	1.9×10^{-25}	4.4×10^{-25}
H_2S	7.3×10^{-3}	3.3×10^{-4}	7.6×10^{-4}
S_2	4.6×10^{-11}	1.0×10^{-11}	1.3×10^{-11}
Ar	0.15	6.6×10^{-3}	1.5×10^{-2}

* Upstream of final desulfidation which is expected to be lower H_2S to 30 ppm
** Temperatures and pressures supplied by METC.

Table 13: Rationale for Selecting Representative Values for NaCl and KCl

Sodium and Potassium Distribution in U.S. Coals

	Range	Arithmetic Mean	Geometric Mean
Sodium*	%	%	%
Illinois Basin	0 - 0.2	0.05	0.03
Eastern U.S.	0.01 - 0.08	0.04	0.03
Western U.S.	0.01 - 0.60	0.14	0.06
Potassium*			
Illinois Basin	0.04 - 0.56	0.17	0.16
Eastern U.S.	0.06 - 0.68	0.25	0.21
Western U.S.	0.01 - 0.32	0.05	0.03

Assume that vapor pressures of NaCl and KCl will be the determining factors.

Vapor Pressure of: NaCl at 1100°F is 1×10^{-6} atmospheric
KCl at 1100°F is ~2.75×10^{-6} atmospheric

Add 2x the level indicated.

If the flow rate of gas is 4 l/min to provide a face velocity of 0.5 ft/min then:

For NaCl = 2ppm (vol) or 0.2×10^{-4} g/min
For KCl =5.5ppm(vol) or 0.7×10^{-4} g/mi

APPENDIX IV: GRAPHS OF SHORT-TERM EXPOSURE DATA

Change in Mass

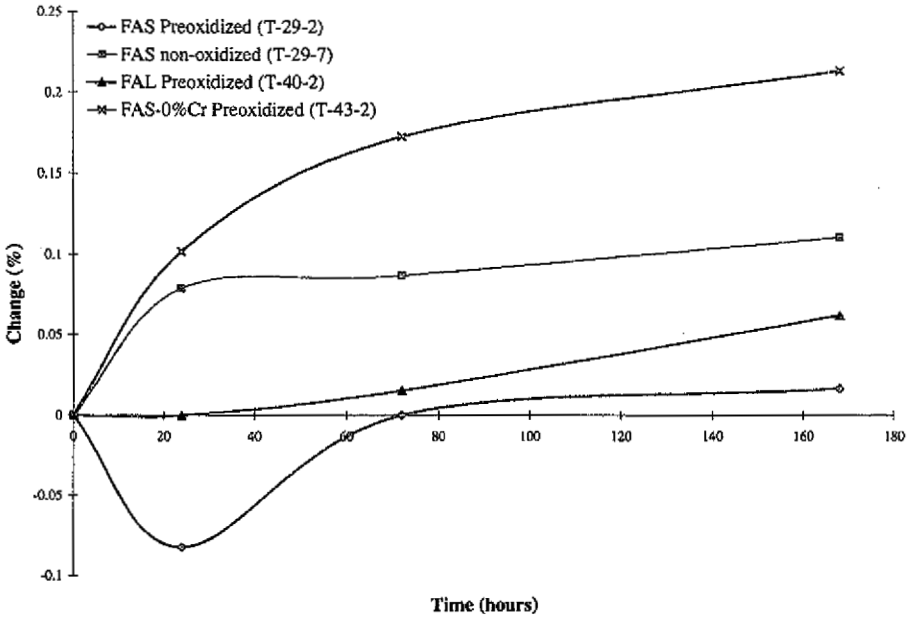

Figure 5: Change in mass of short-term Exposure Run 1 samples. Exposed to 925°F with 0.0783 vol% H_2S at 1 atm. Data points from 336 hours (14 days) are unavailable.

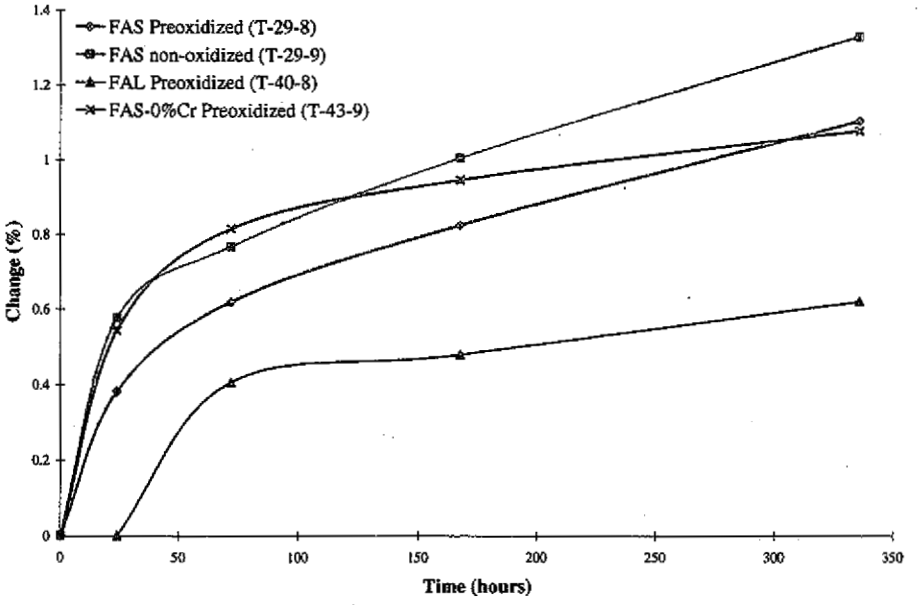

Figure 6: Change in mass of short-term Exposure Run 2 samples. Exposed to 1200°F with 0.783 vol% H_2S at 1 atm.

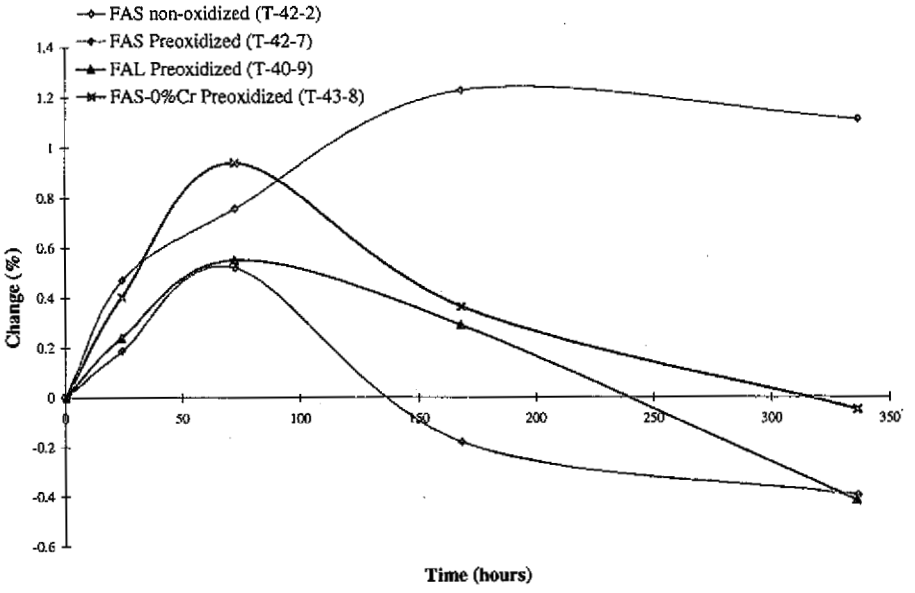

Figure 7: Change in mass of short-term Exposure Run 3 samples. Exposed to 925°F with 7.83 vol% H_2S at 1 atm.

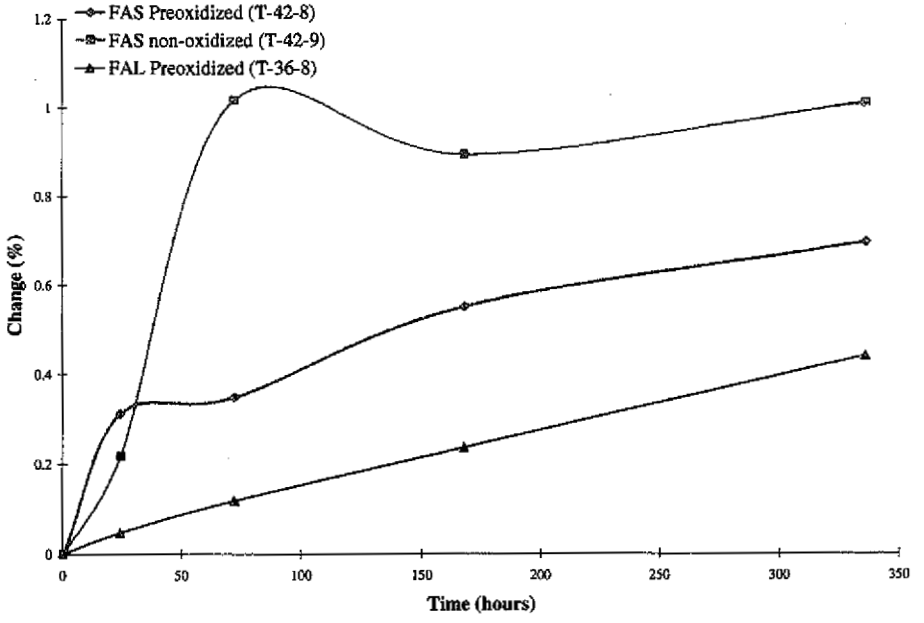

Figure 8: Change in mass of short-term Exposure Run 4 samples. Exposed to 925°F with 0.783 vol% H_2S at 1 atm.

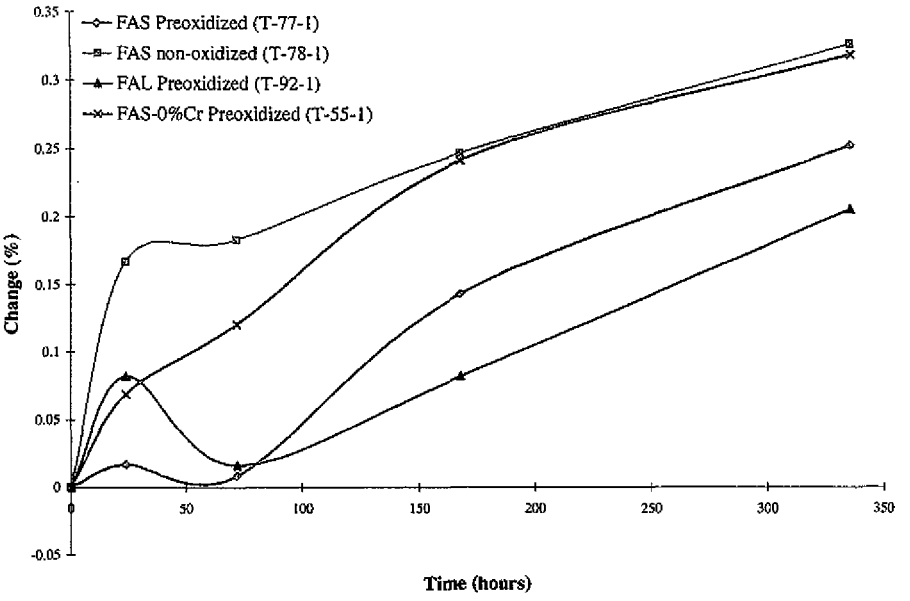

Figure 9: Change in mass of short-term Exposure Run 5 samples. Exposed to 1050°F with 0.0783 vol% H_2S at 1 atm.

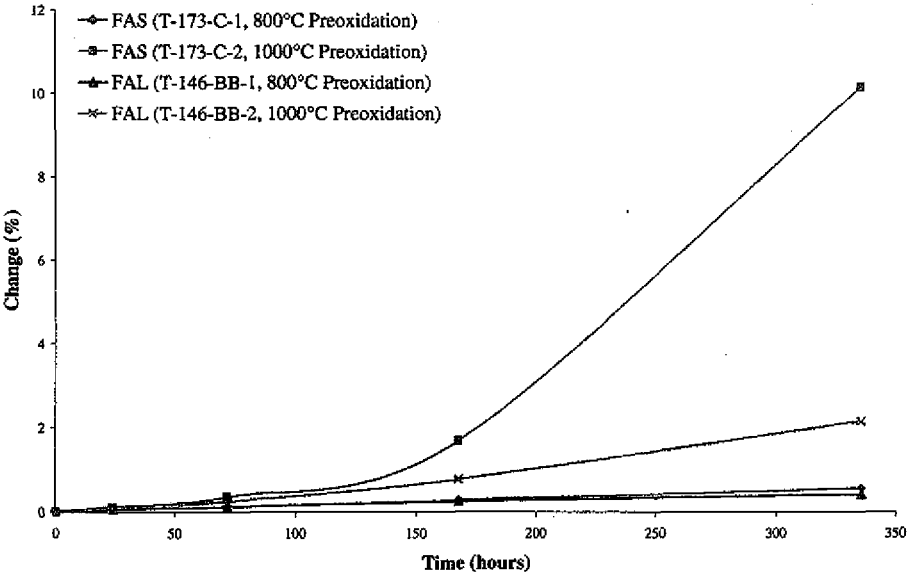

Figure 10: Change in mass of short-term Exposure Run 6 samples. Exposed to 1200°F with 7.83 vol% H_2S at 1 atm. Plot is dominated by the large mass gains of the 1000°C preoxidized samples. Figure 11 plots only the 800°C preoxidized samples.

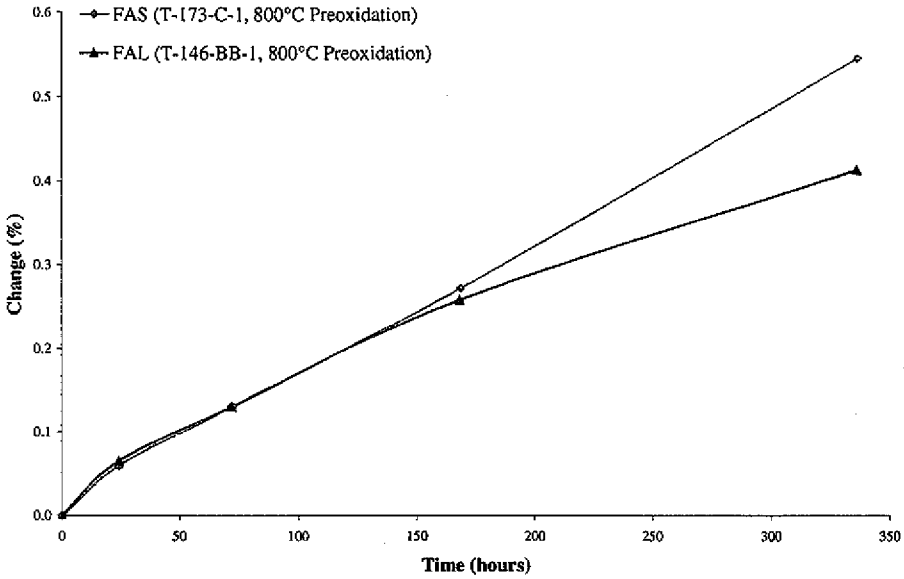

Figure 11: Change in mass of short-term Exposure Run 6 samples. Exposed to 1200°F with 7.83 vol% H2S at 1 atm.

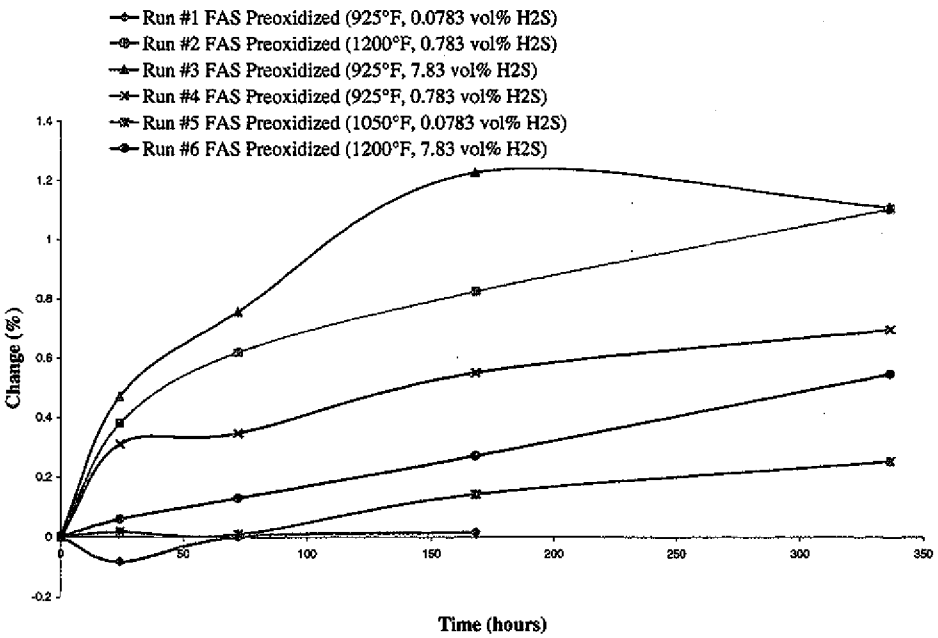

Figure 12: Comparison of the mass gains of the FAS preoxidized (800°C) samples.

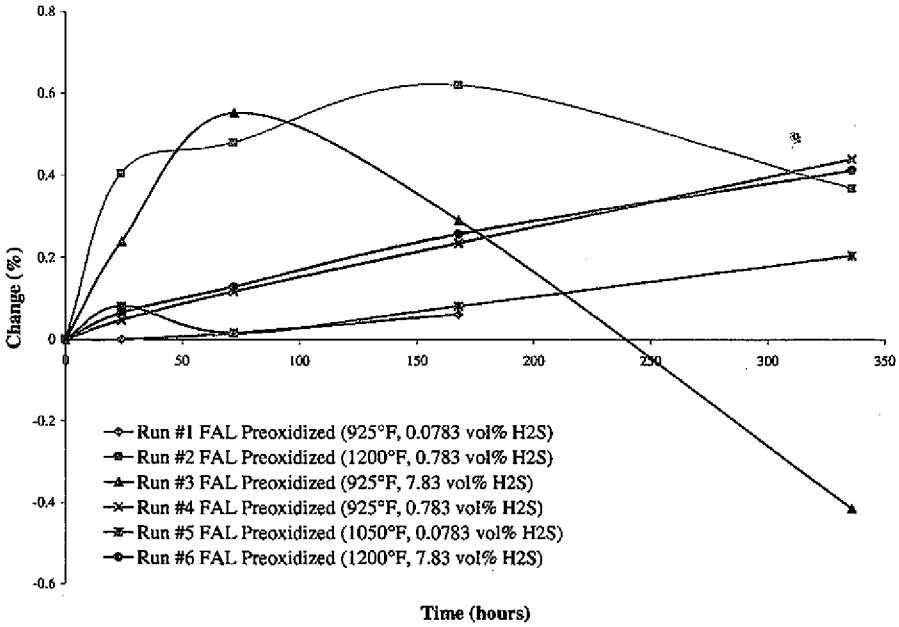

Figure 13: Comparison of the mass gains of the FAL preoxidized (800°C) samples.

Change in Pressure Drop

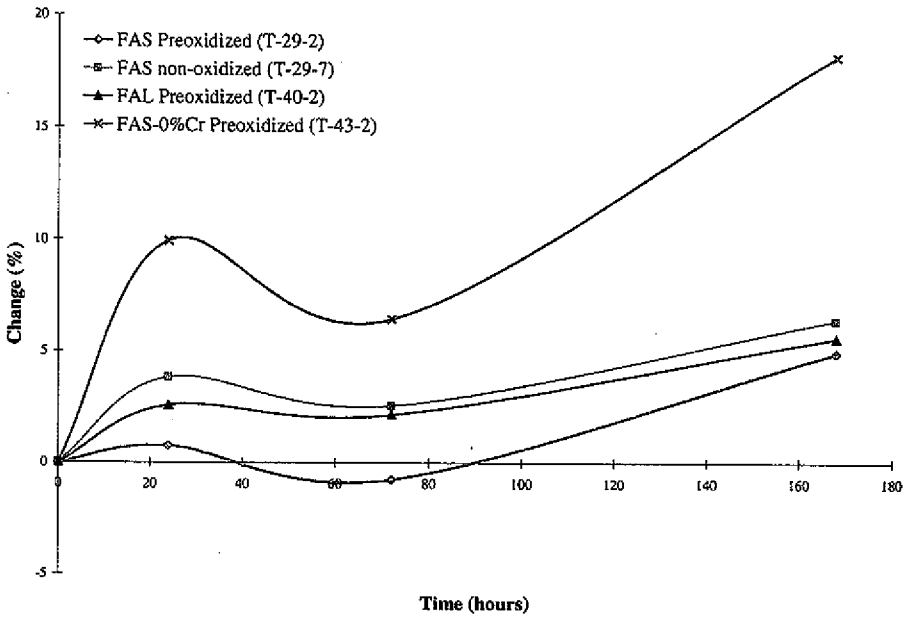

Figure 14: Change in pressure drop of short-term Exposure Run 1 samples. Exposed to 925°F with 0.0783 vol% H_2S at 1 atm. Data points for 336 hours (14 days) are unavailable.

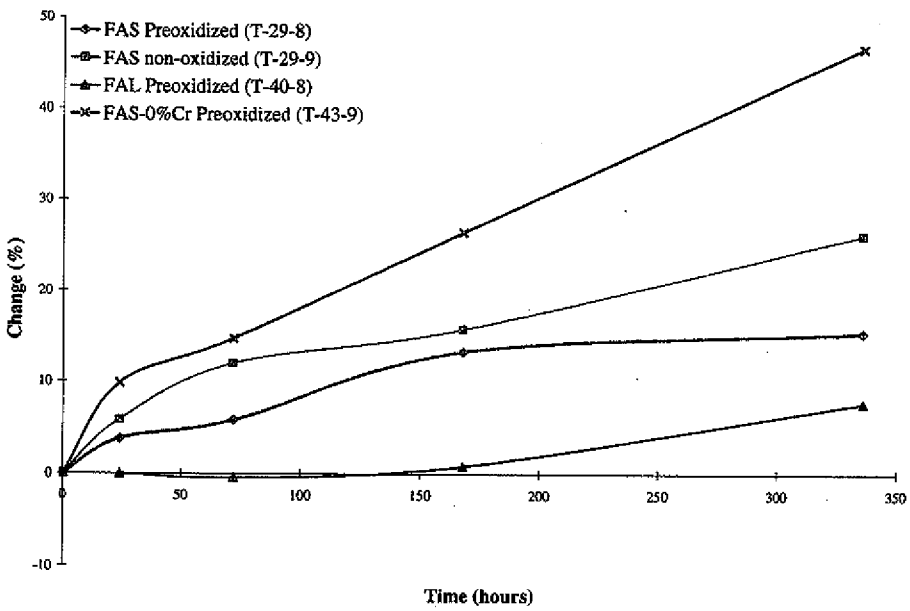

Figure 15: Change in pressure drop of short-term Exposure Run 2 samples. Exposed to 1200°F with 0.783 vol% H_2S at 1 atm.

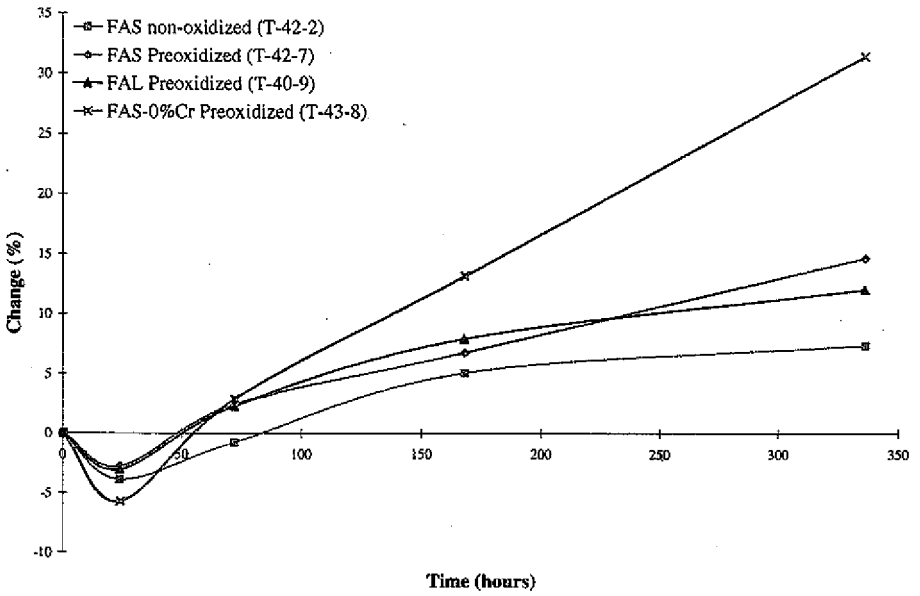

Figure 16: Change in pressure drop of short-term Exposure Run 3 samples. Exposed to 925°F with 7.83 vol% H_2S at 1 atm.

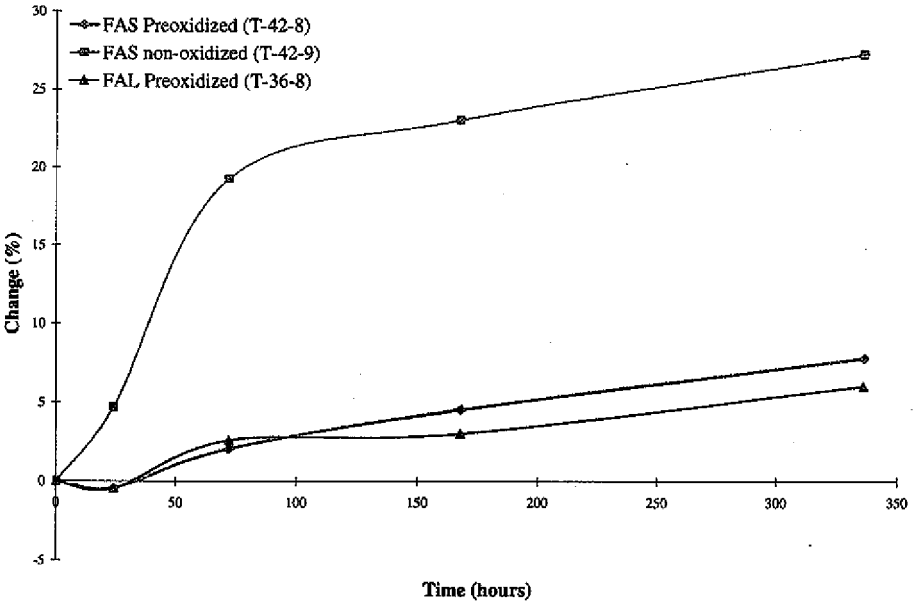

Figure 17: Change in pressure drop of short-term Exposure Run 4 samples. Exposed to 925°F with 0.783 vol% H_2S at 1 atm.

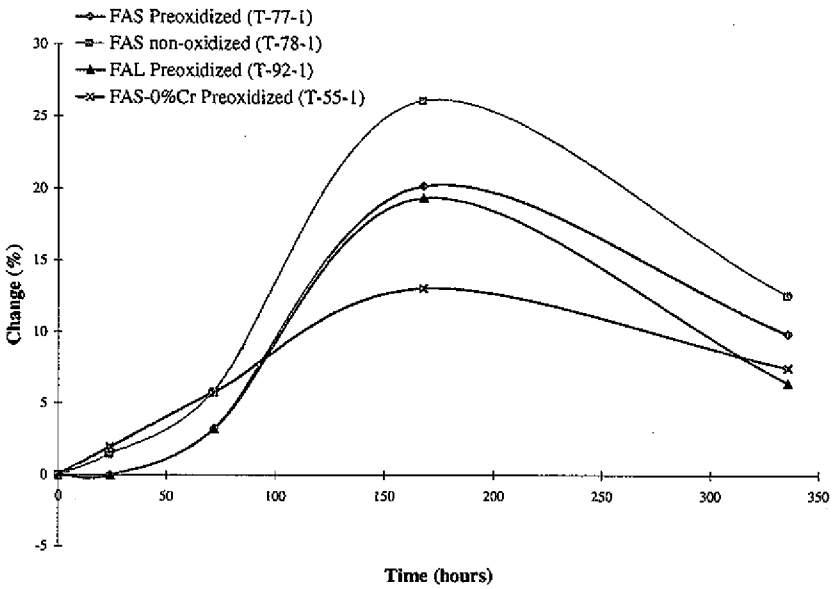

Figure 18: Change in pressure drop of short-term Exposure Run 5 samples. Exposed to 1050°F with 0.0783 vol% H_2S at 1 atm.

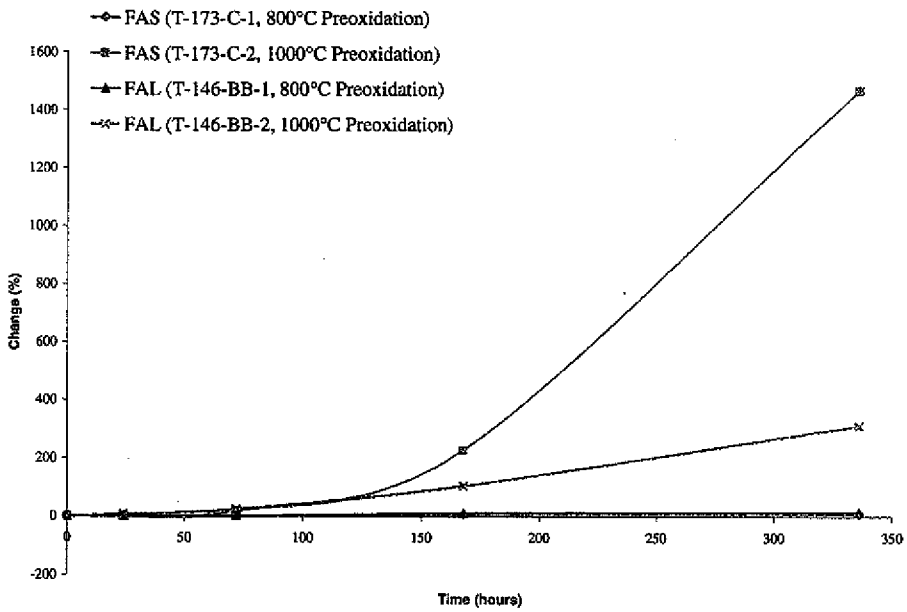

Figure 19: Change in pressure drop of short-term Exposure Run 6 samples. Exposed to 1200°F with 7.83 vol% H_2S at 1 atm. The 800°C preoxidation samples are plotted in .

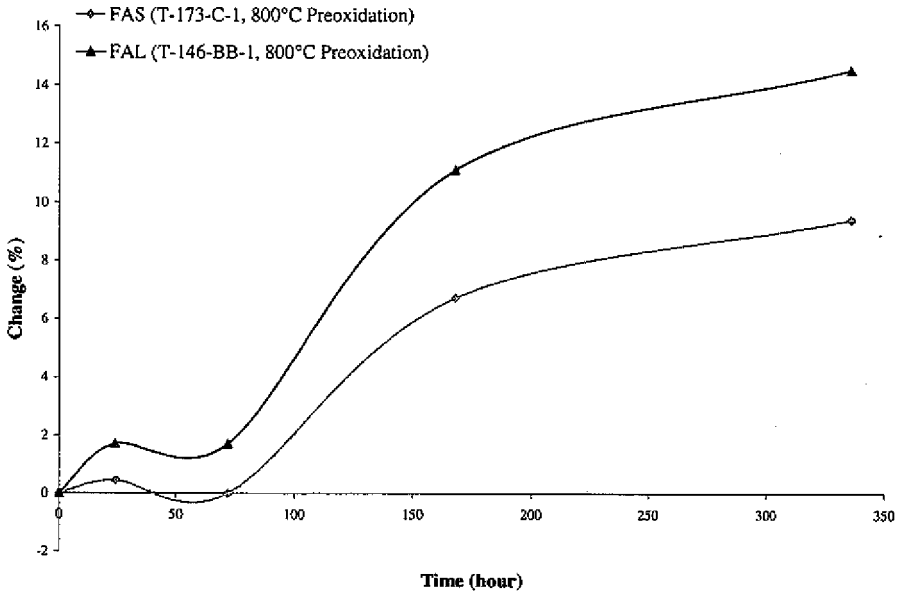

Figure 20: Change in pressure drop of short-term Exposure Run 6 samples. Exposed to 1200°F with 7.83 vol% H2S at 1 atm.

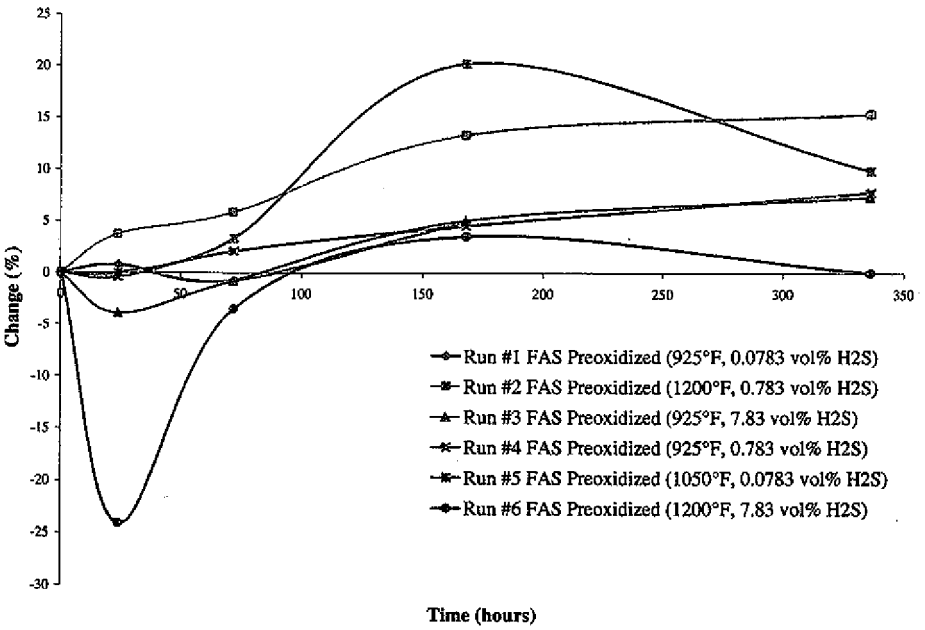

Figure 21: Comparison of pressure drops of the FAS preoxidized (800°C) samples.

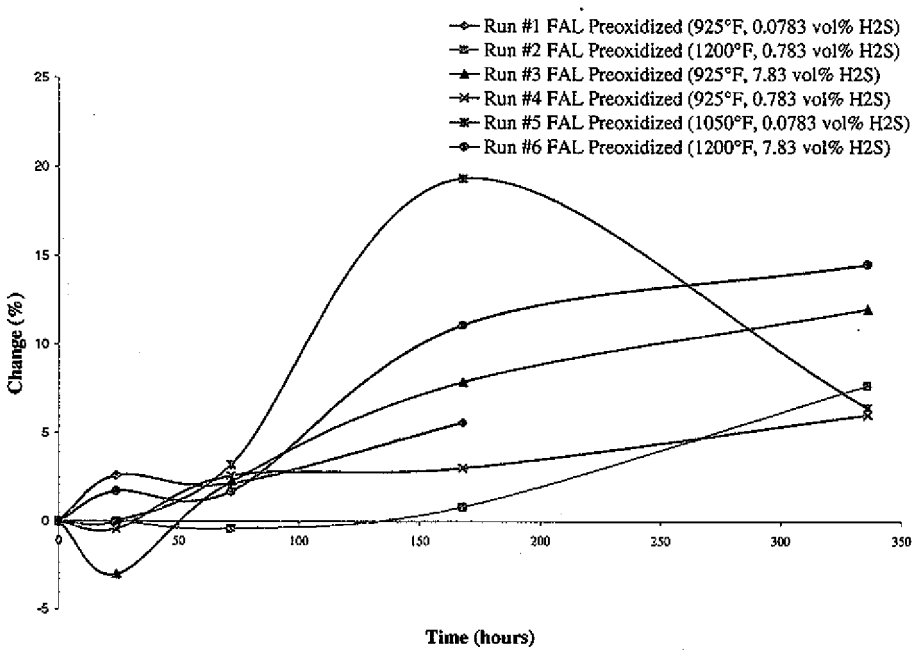

Figure 22: Comparison of pressure drops of the FAL preoxidized (800°C) samples.

Change in Open Bubble Point

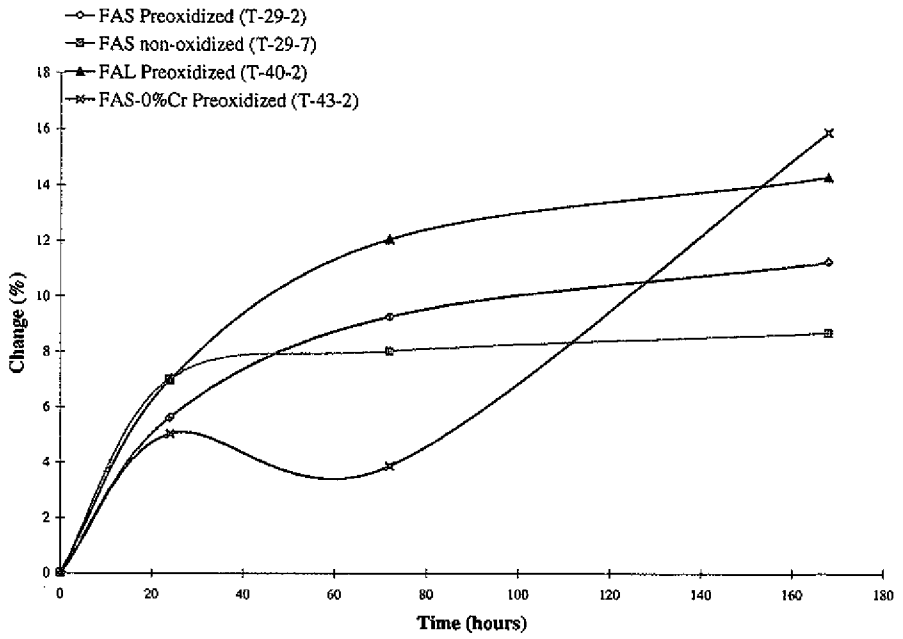

Figure 23: Change in open bubble point of short-term Exposure Run 1 samples. Exposed to 925°F with 0.0783 vol% H_2S at 1 atm. Data points from 336 hours (14 days) are unavailable.

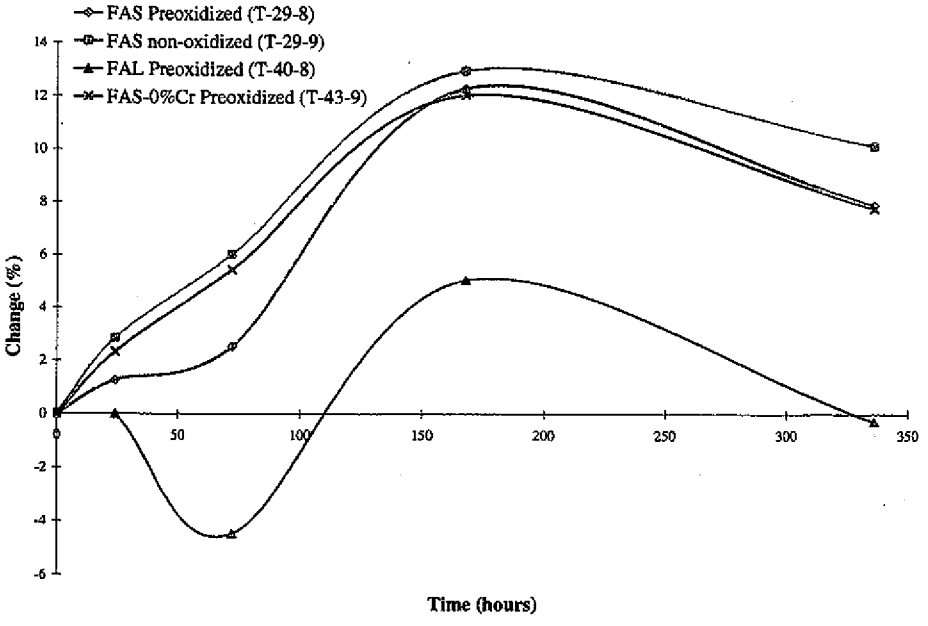

Figure 24: Change in open bubble point of short-term Exposure Run 2 samples. Exposed to 1200°F with 0.783 vol% H_2S at 1 atm.

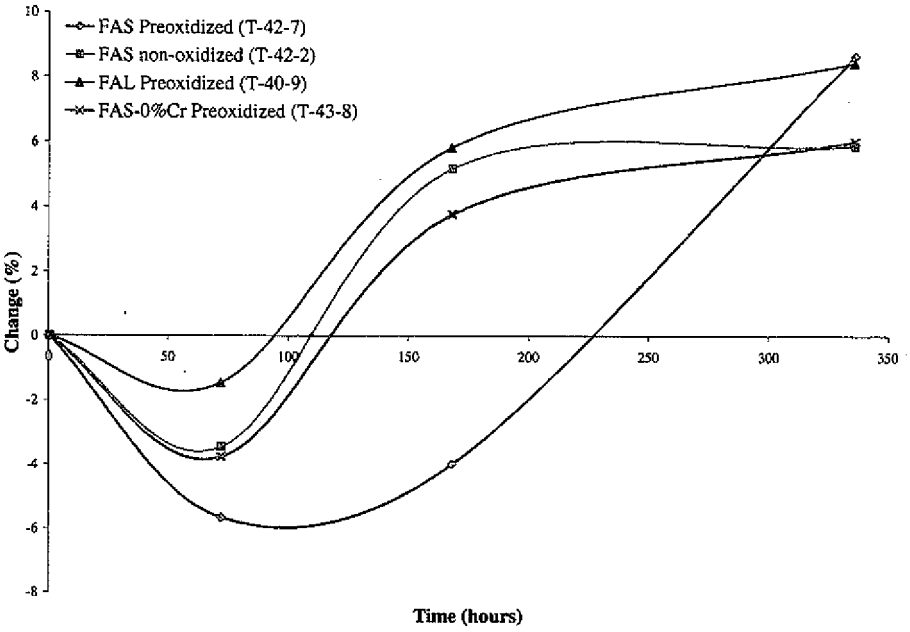

Figure 25: Change in open bubble point of short-term Exposure Run 3 samples. Exposed to 925°F with 7.83 vol% H_2S at 1 atm.

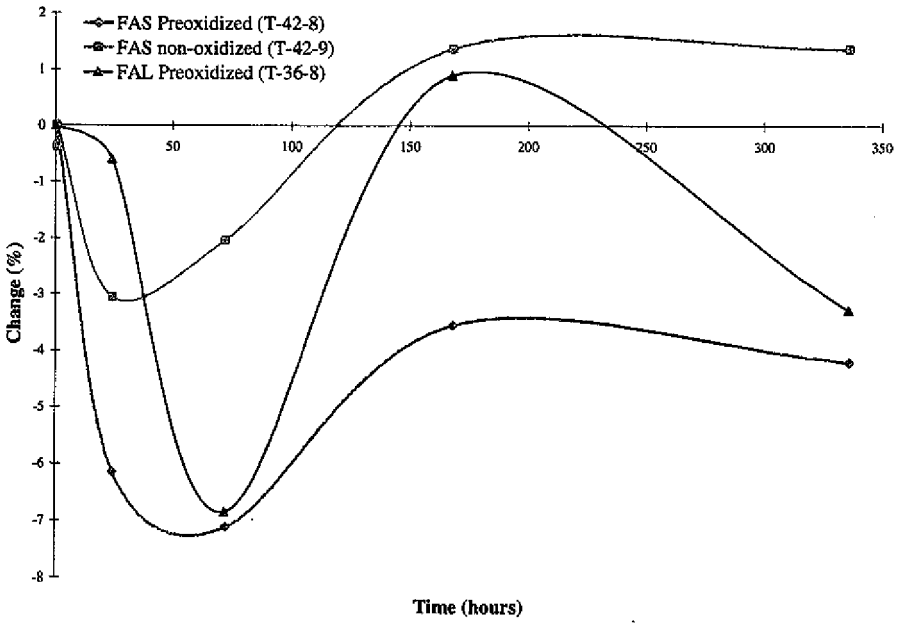

Figure 26: Change in open bubble point of short-term Exposure Run 4 samples. Exposed to 925°F with 0.783 vol% H_2S at 1 atm.

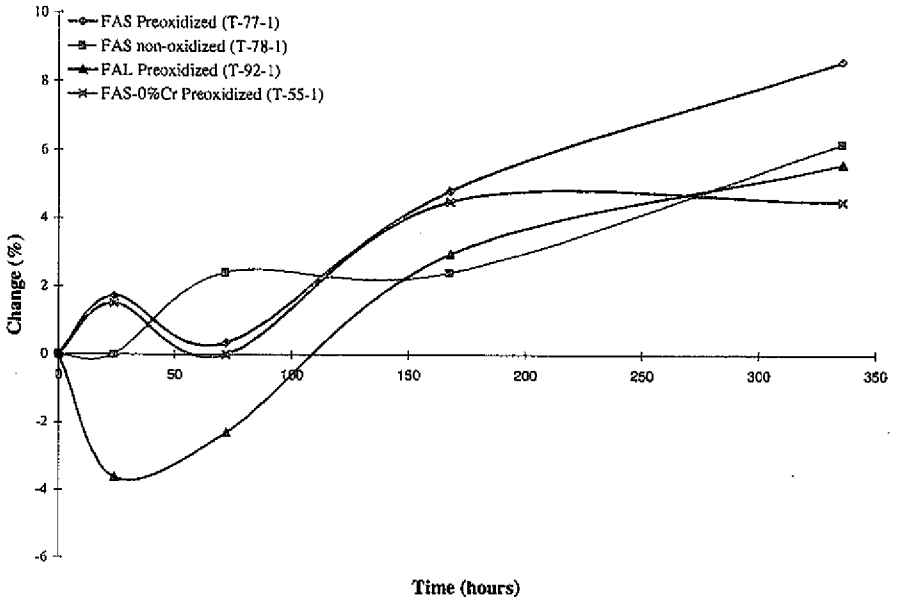

Figure 27: Change in open bubble point of short-term Exposure Run 5 samples. Exposed to 1050°F with 0.0783 vol% H_2S at 1 atm.

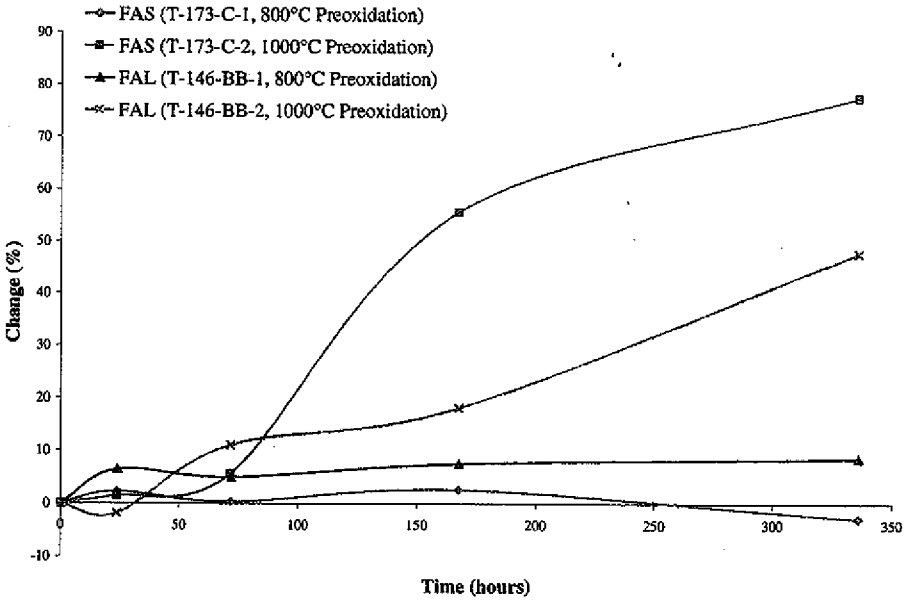

Figure 28: Change in open bubble point of short-term Exposure Run 6 samples. Exposed to 1200°F with 7.83 vol% H_2S at 1 atm.

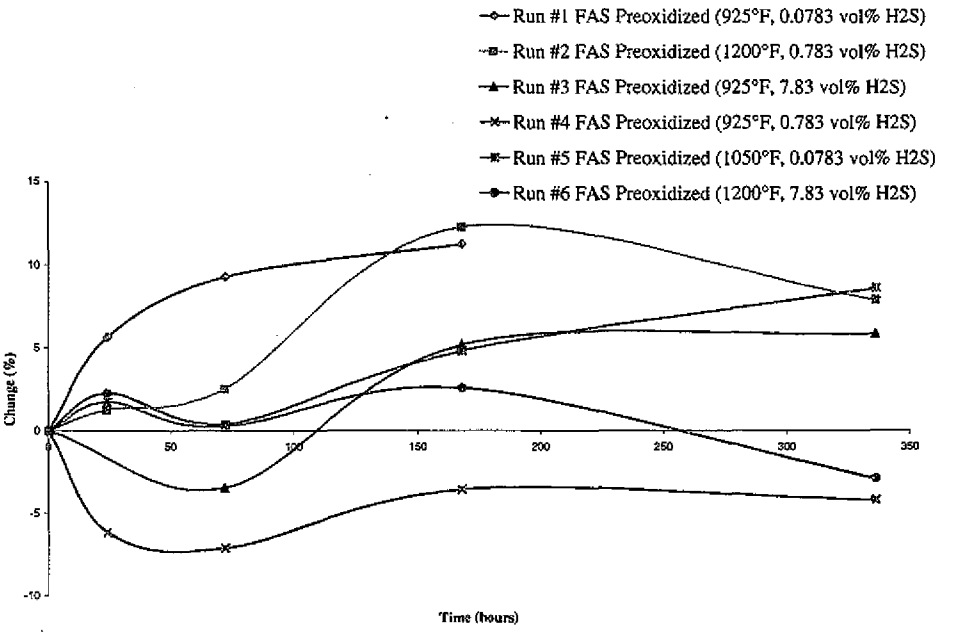

Figure 29: Comparison of the open bubble point of the FAS preoxidized (800°C) alloys.

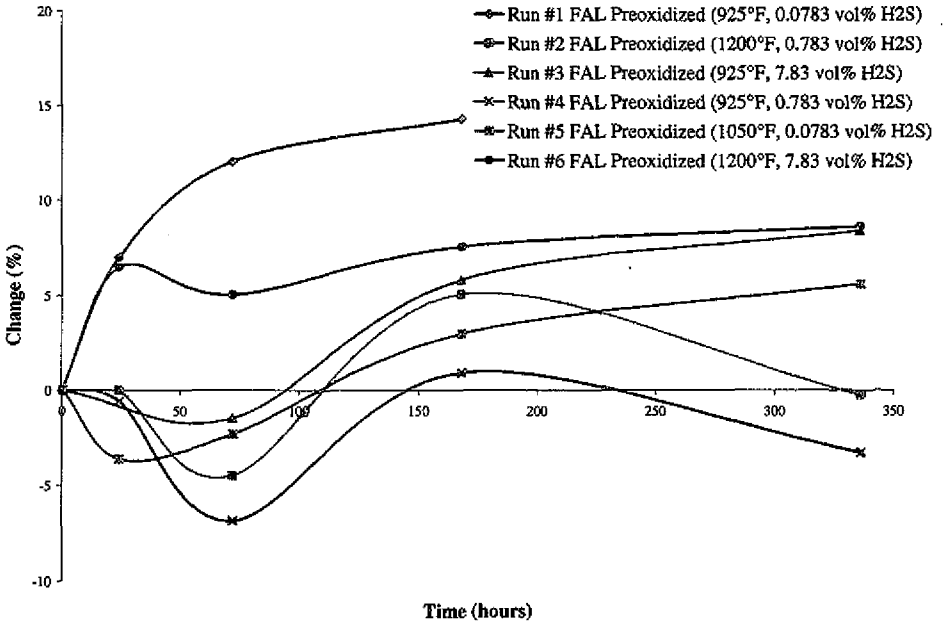

Figure 30: Comparison of the open bubble point of the FAL preoxidized (800°C) alloys.

Change in First Bubble Point

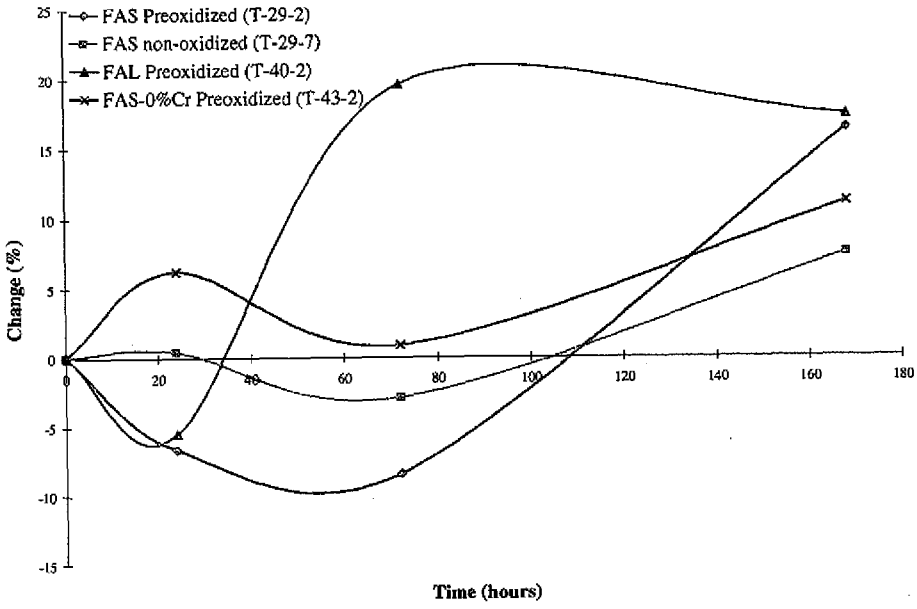

Figure 31: Change in the first bubble point of short-term Exposure Run 1 samples. Exposed to 925°F with 0.0783 vol% H_2S at 1 atm. Data points for 336 hours (14 days) are unavailable.

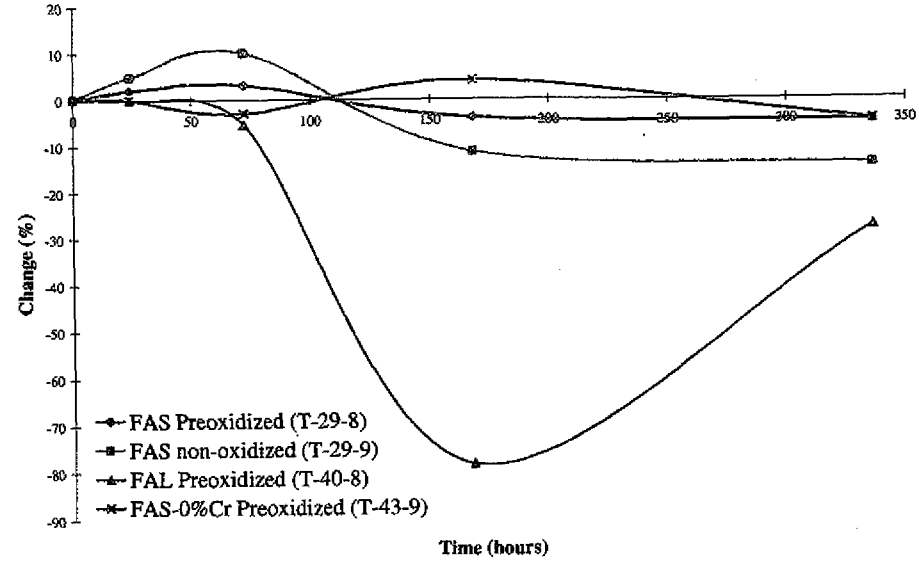

Figure 32: Change in the first bubble point of short-term Exposure Run 2 samples. Exposed to 1200°F with 0.783 vol% H_2S at 1 atm.

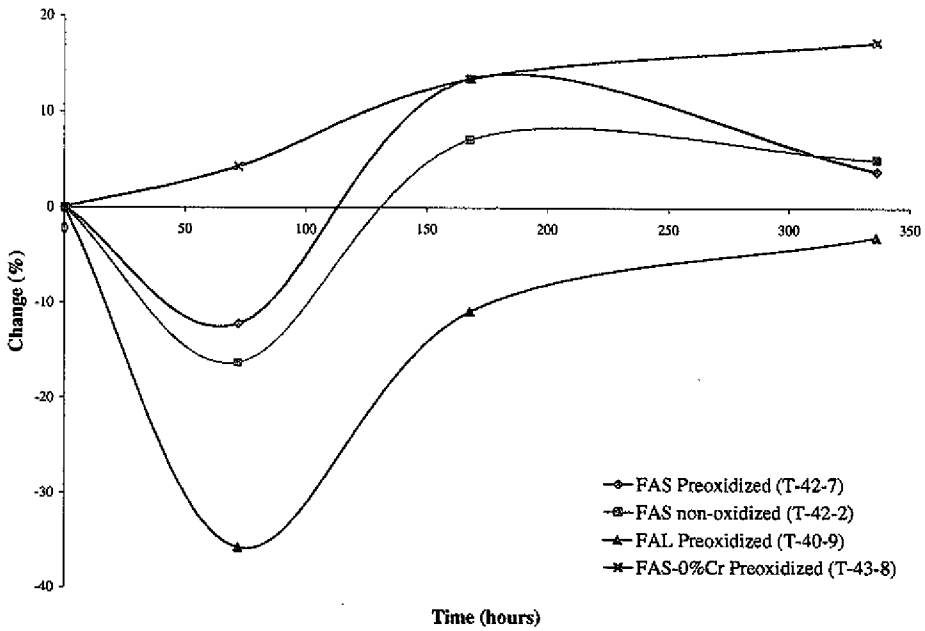

Figure 33: Change in the first bubble point of short-term Exposure Run 3 samples. Exposed to 925°F with 7.83 vol% H_2S at 1 atm.

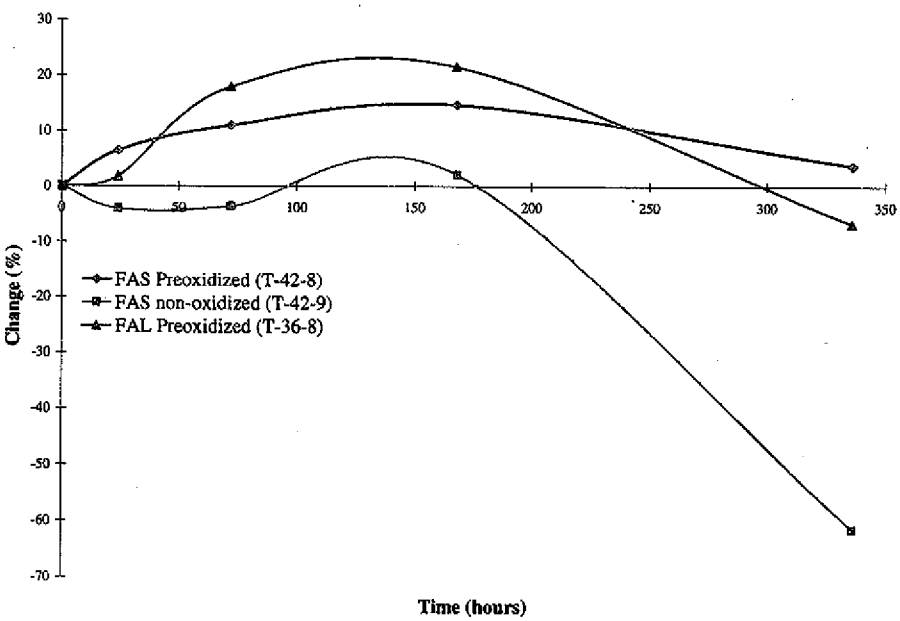

Figure 34: Change in the first bubble point of short-term Exposure Run 4 samples. Exposed to 925°F with 0.783 vol% H_2S at 1 atm.

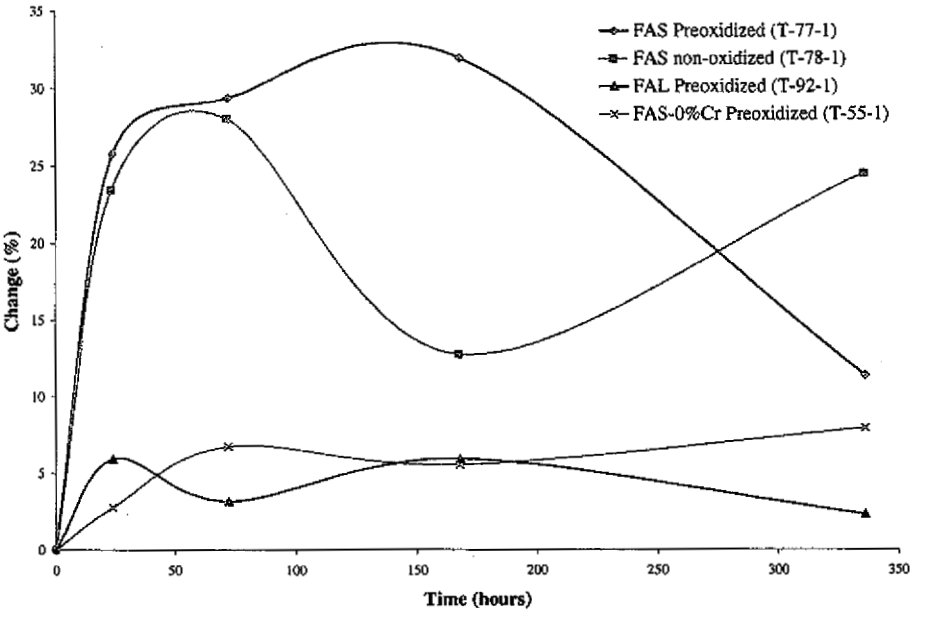

Figure 35: Change in the first bubble point of short-term Exposure Run 5 samples. Exposed to 1050°F with 0.0783 vol% H_2S at 1 atm.

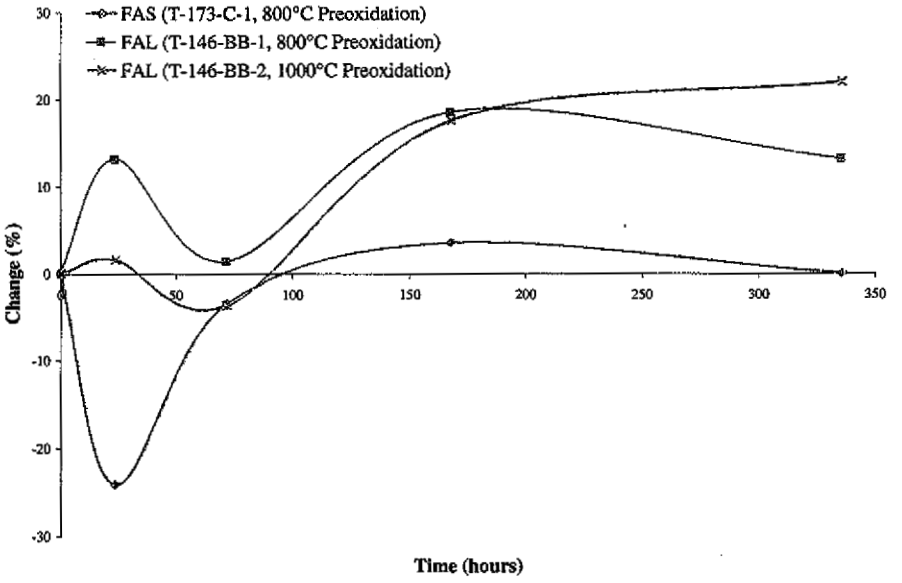

Figure 36: Change in the first bubble point of short-term Exposure Run 6 samples. Exposed to 1200°F with 7.83 vol% H_2S at 1 atm. FAL sample preoxidized had a logntitudinal crack preventing it from being tested.

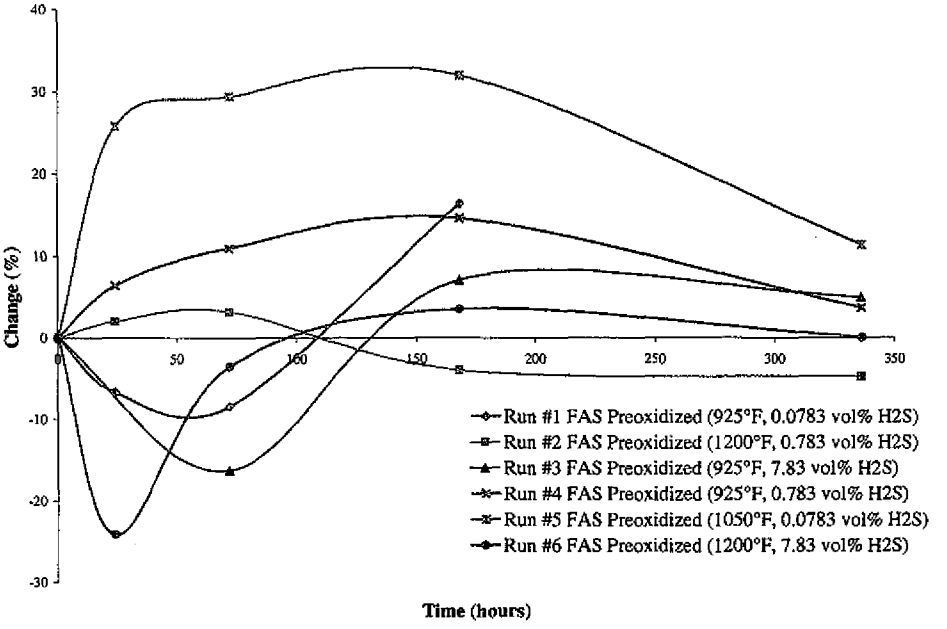

Figure 37: Comparison of the FAS preoxidized (800°C) first bubble points.

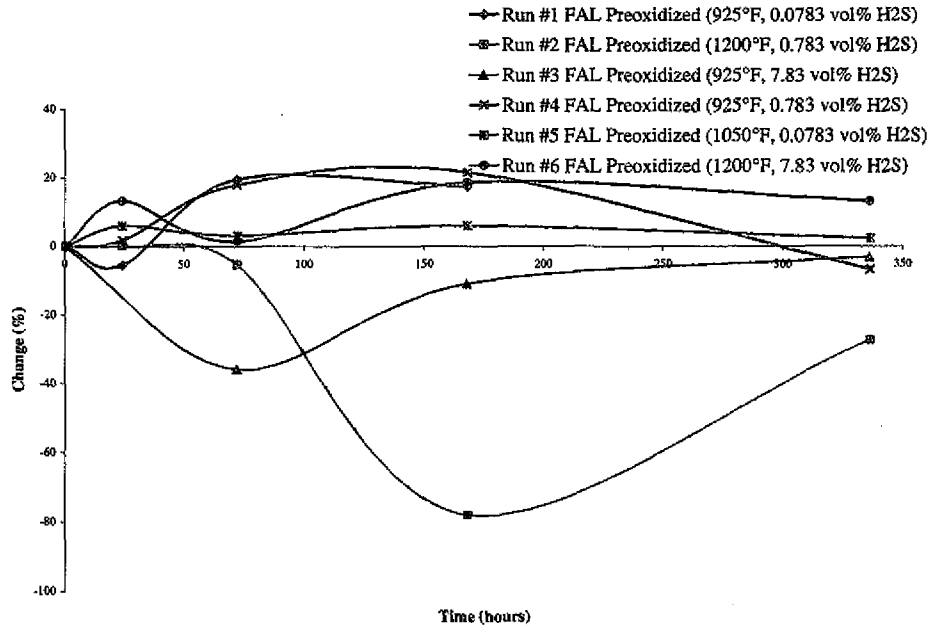

Figure 38: Comparison of the FAL preoxidized (800°C) first bubble points.

Change in Tenth Bubble Point

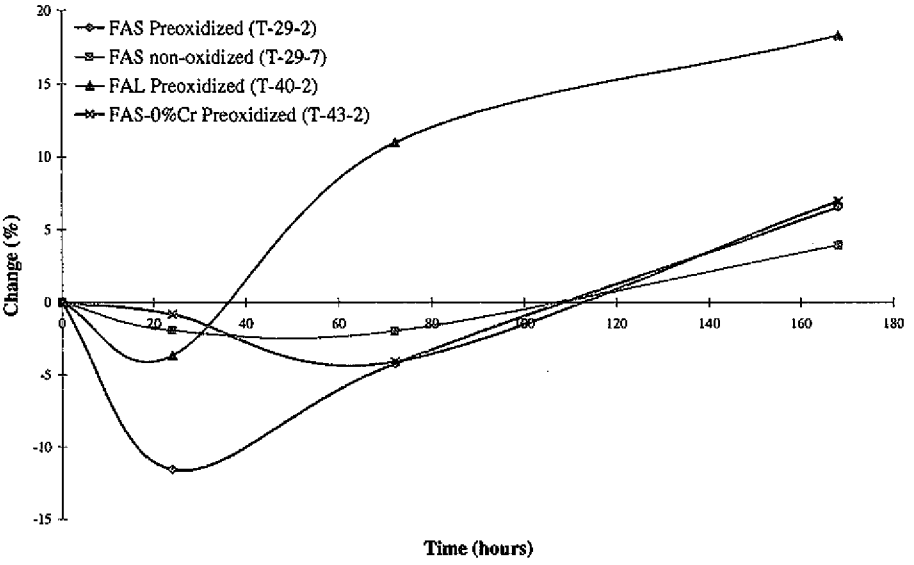

Figure 39: Change in the tenth bubble point of short-term Exposure Run 1 samples. Exposed to 925°F with 0.0783 vol% H_2S at 1 atm. Data points for 336 hours (14 days) are unavailable.

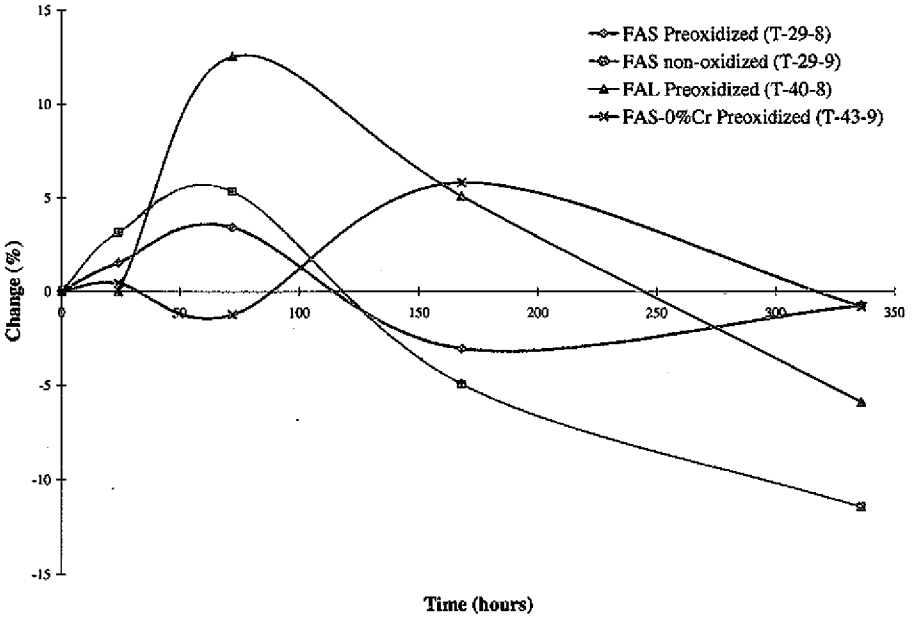

Figure 40: Change in the tenth bubble point of short-term Exposure Run 2 samples. Exposed to 1200°F with 0.783 vol% H_2S at 1 atm.

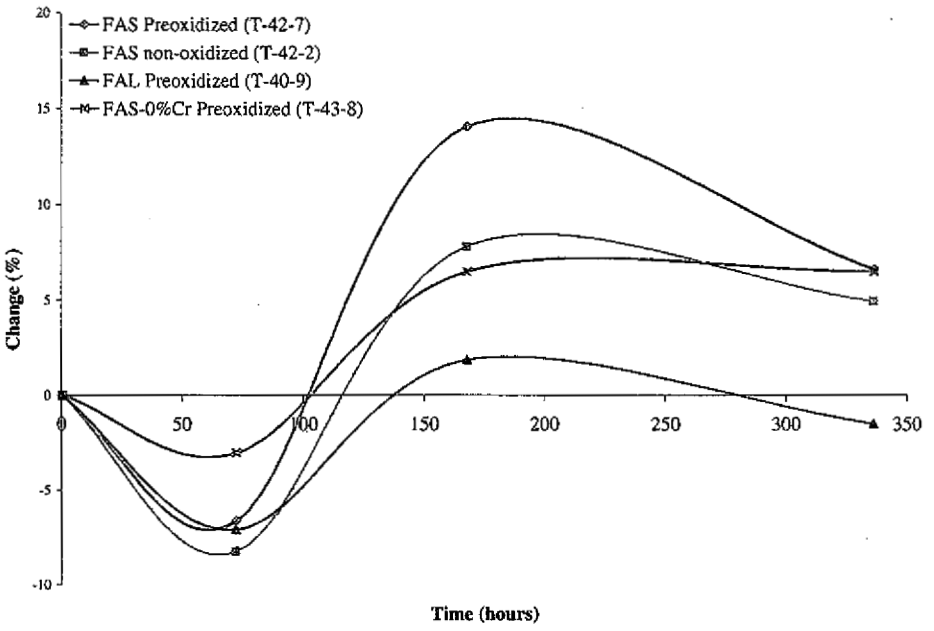

Figure 41: Change in the tenth bubble point of short-term Exposure Run 3 samples. Exposed to 925°F with 7.83 vol% H_2S at 1 atm.

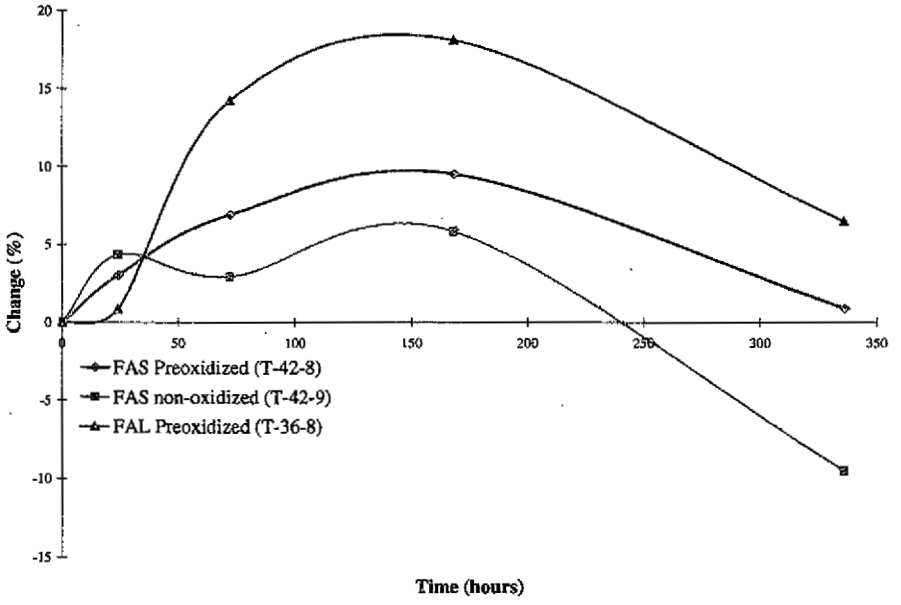

Figure 42: Change in the tenth bubble point of short-term Exposure Run 4 samples. Exposed to 925°F with 0.0783 vol% H_2S at 1 atm.

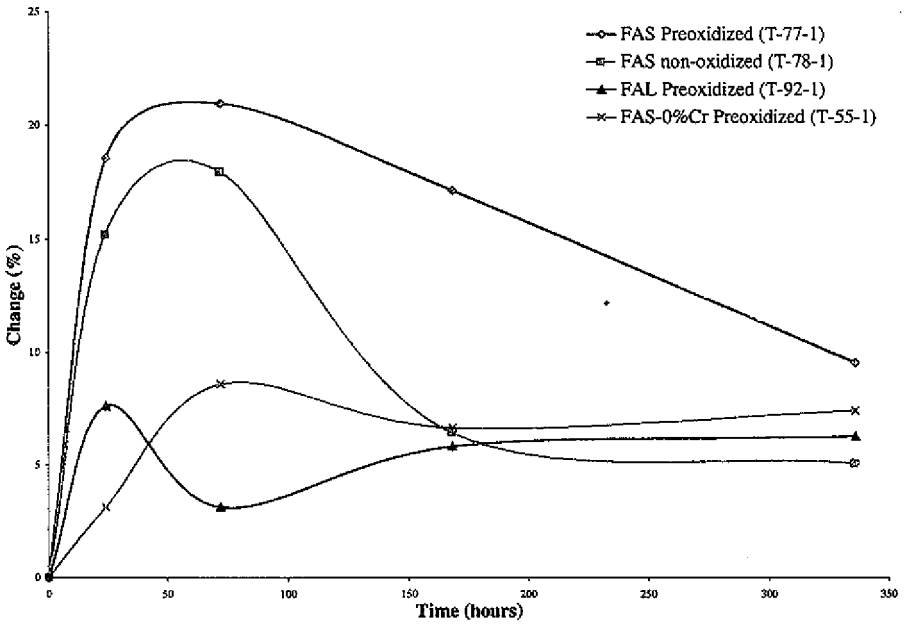

Figure 43: Change in the tenth bubble point of short-term Exposure Run 5 samples. Exposed to 925°F with 0.0783 vol% H_2S at 1 atm.

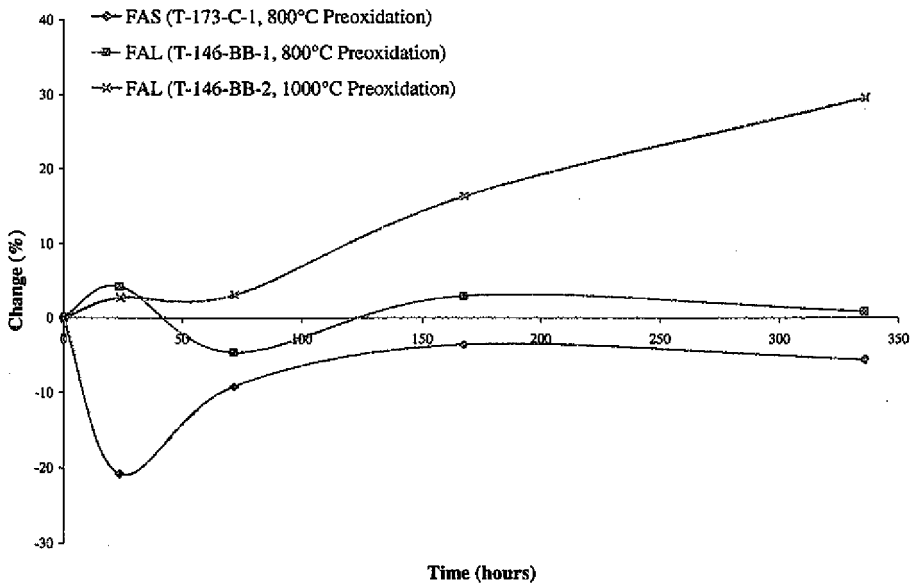

Figure 44: Change in the tenth bubble point of short-term Exposure Run 6 samples. Exposed to 1200°F with 7.83 vol% H_2S at 1 atm.

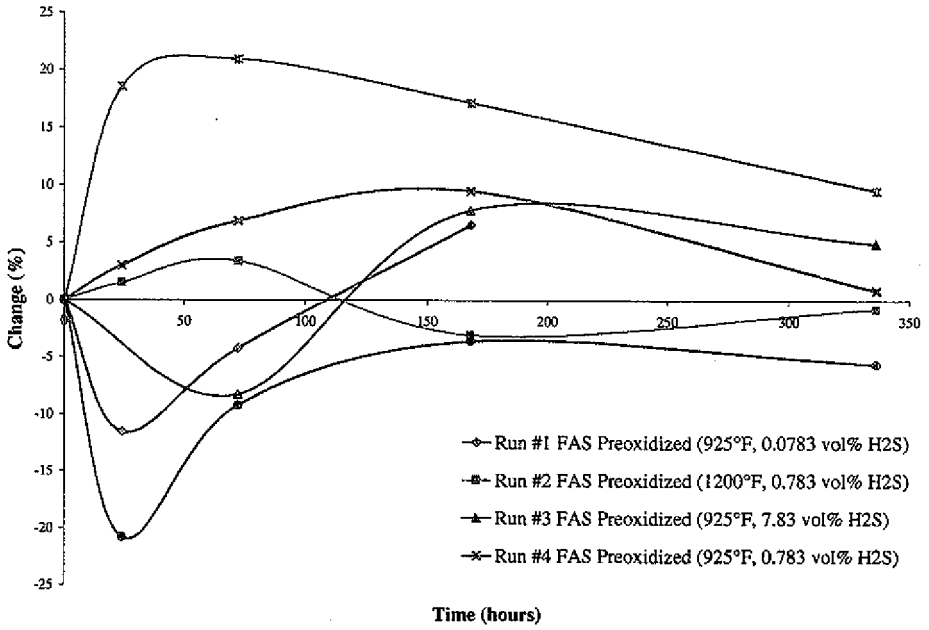

Figure 45: Comparison of the tenth bubble point of the FAS preoxidized (800°C) samples.

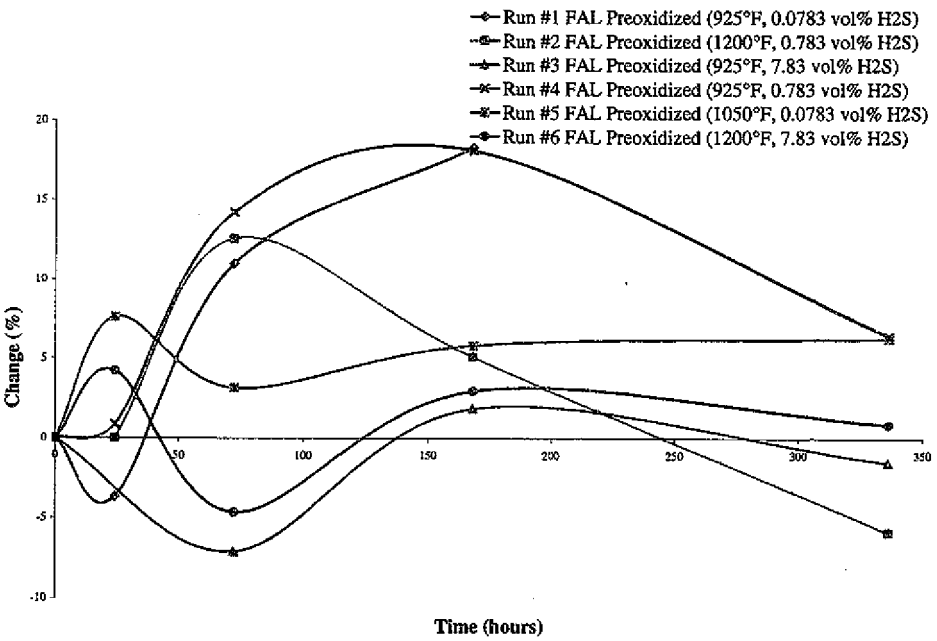

Figure 46: Comparison of the tenth bubble point of the FAL preoxidized (800°C) samples

Additional Graphs of Short-term Exposure Data

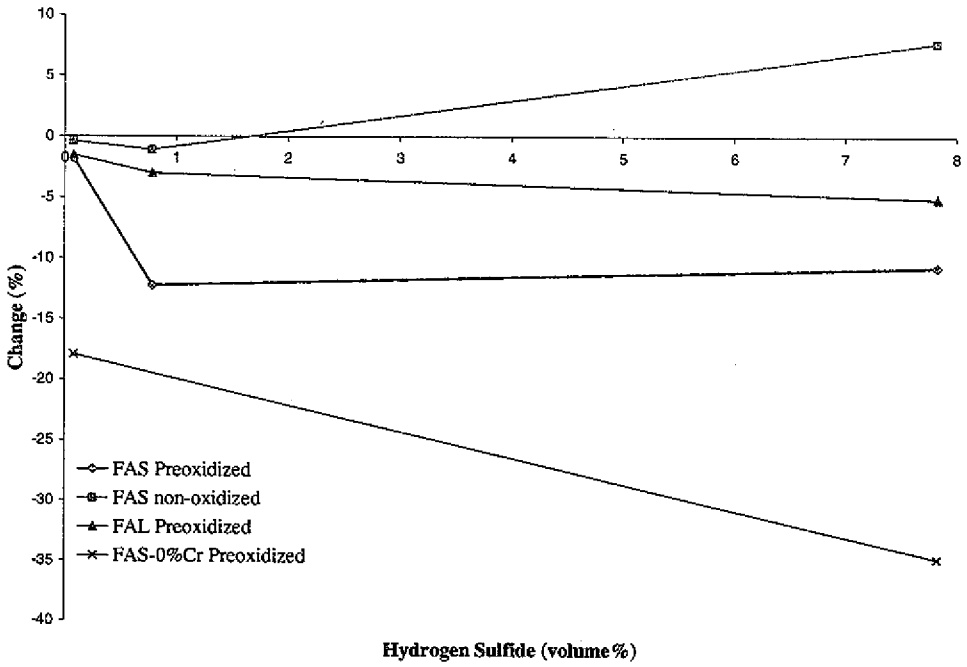

Figure 47: Change in the carbon content versus the exposure levels of hydrogen sulfide at 925°F.

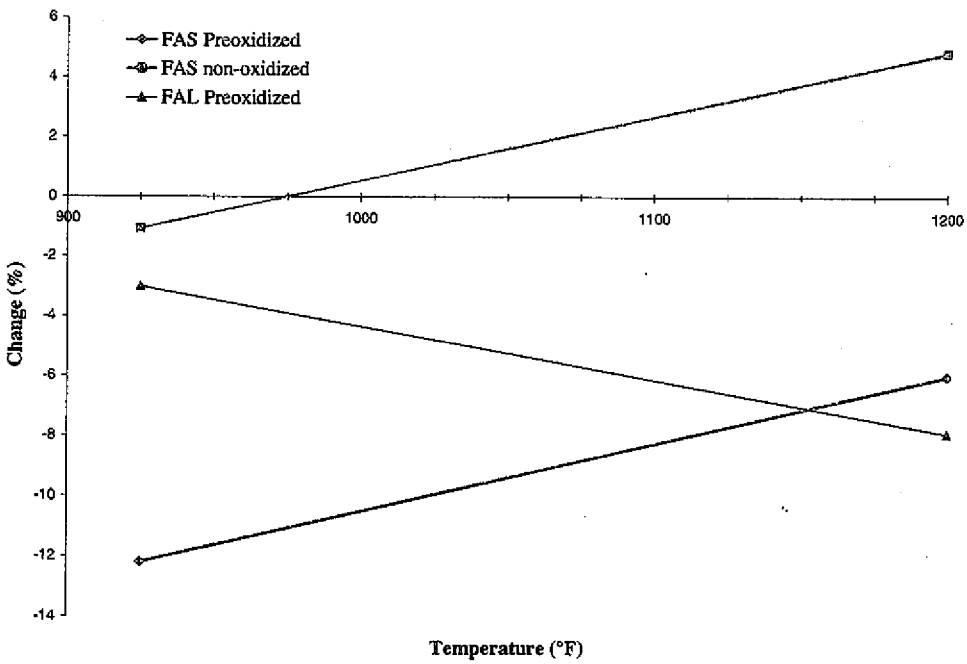

Figure 48: Change in the carbon content versus exposure temperature with 0.783 vol% hydrogen sulfide.

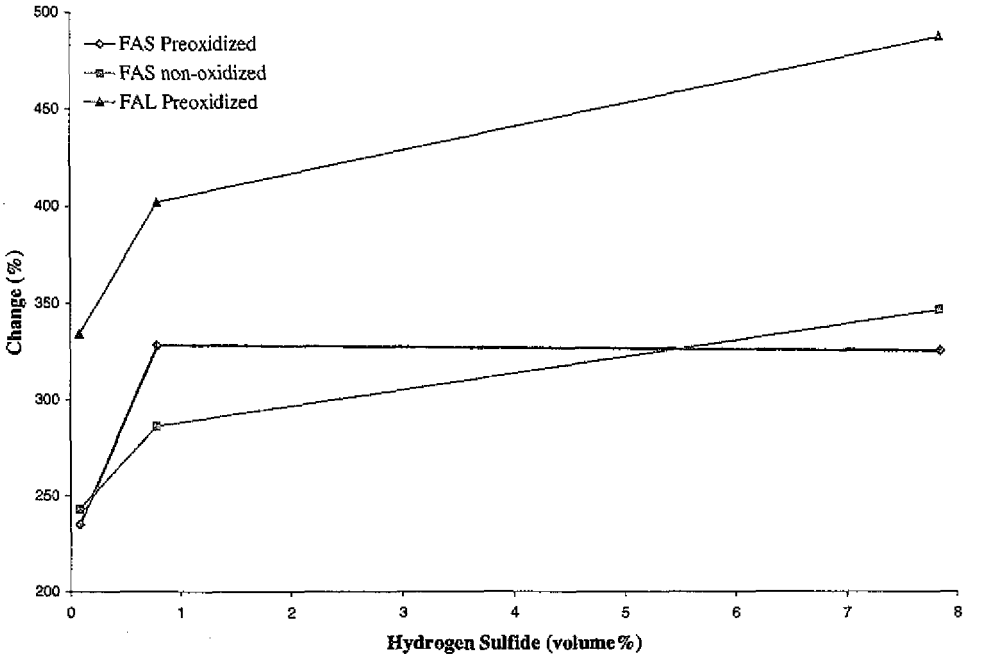

Figure 49: Change in sulfur content versus exposure levels of hydrogen sulfide at 925°F.

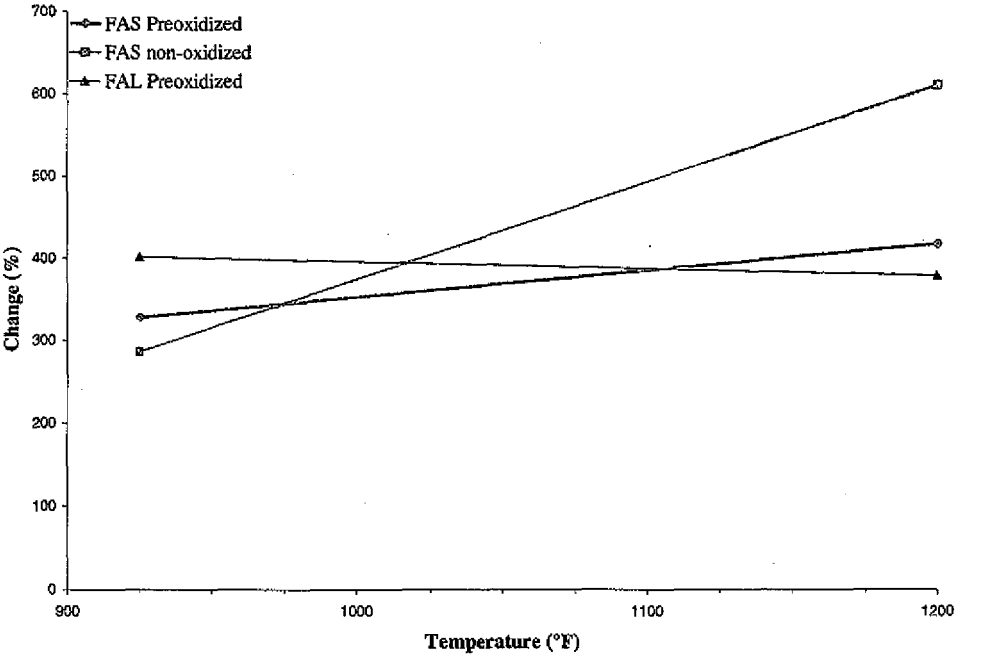

Figure 50: Change in sulfur content versus exposure temperature with 0.783 vol% hydrogen sulfide.

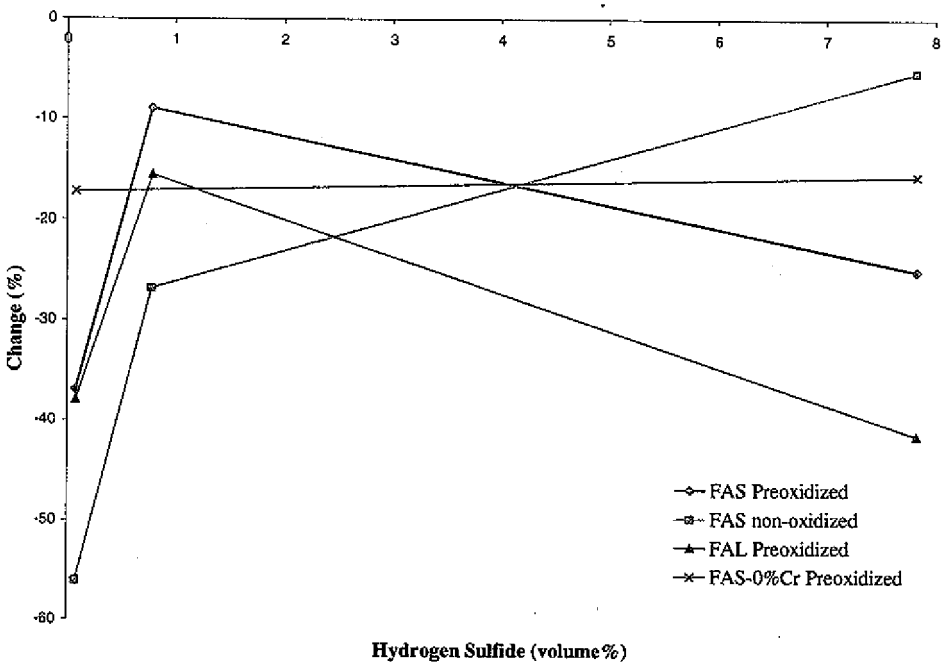

Figure 51: Change in ductility versus the exposure level of hydrogen sulfide at 925°F.

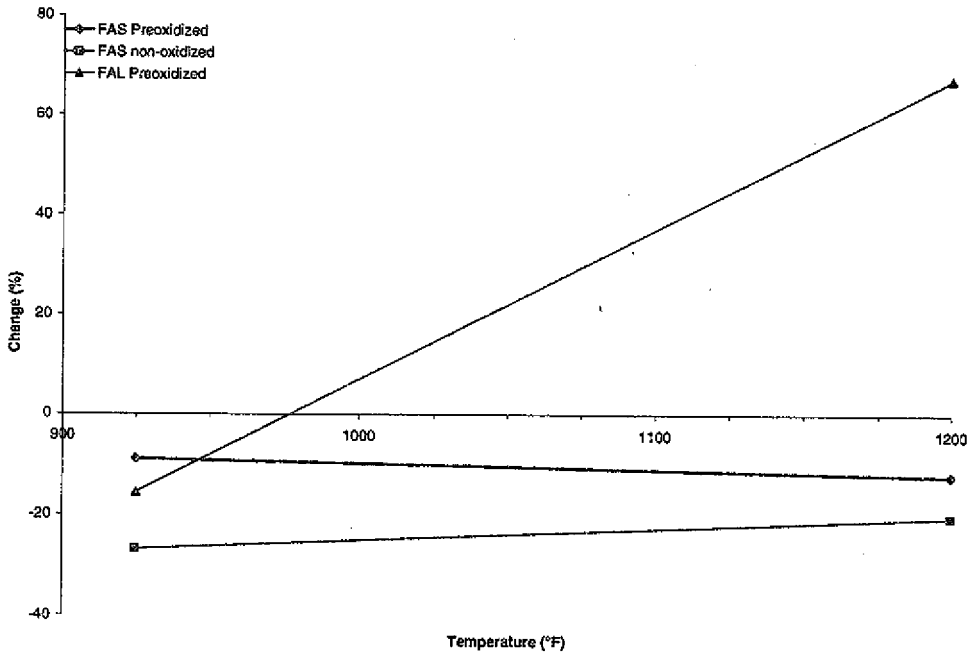

Figure 52: Change in ductility versus exposure temperature with 0.783 col% hydrogen sulfide.

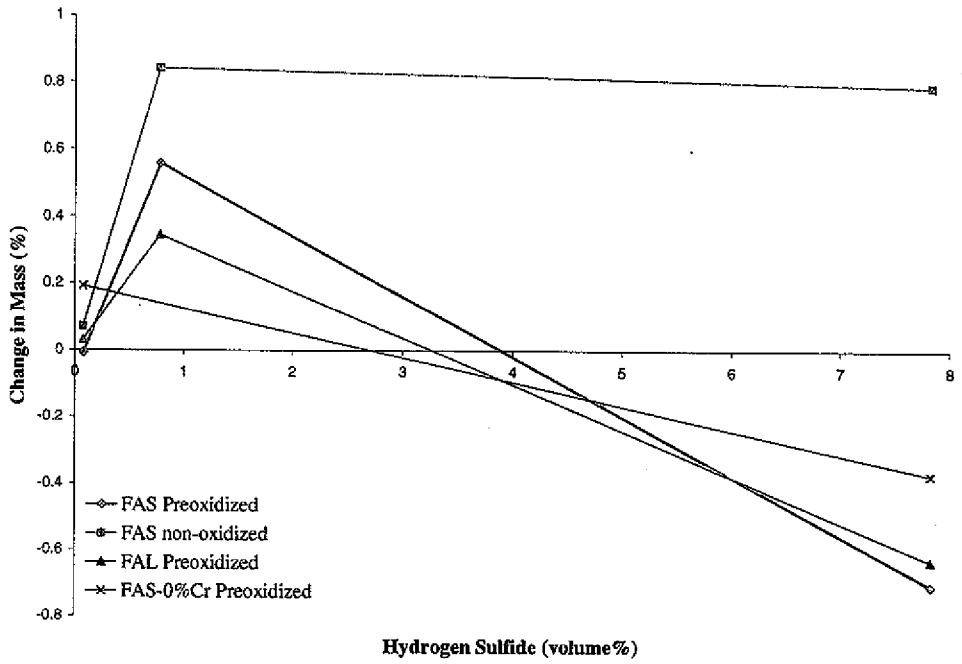

Figure 53: Change in mass versus exposure level of hydrogen sulfide at 925°F. The solid 310SS hardware is affecting the change in mass.

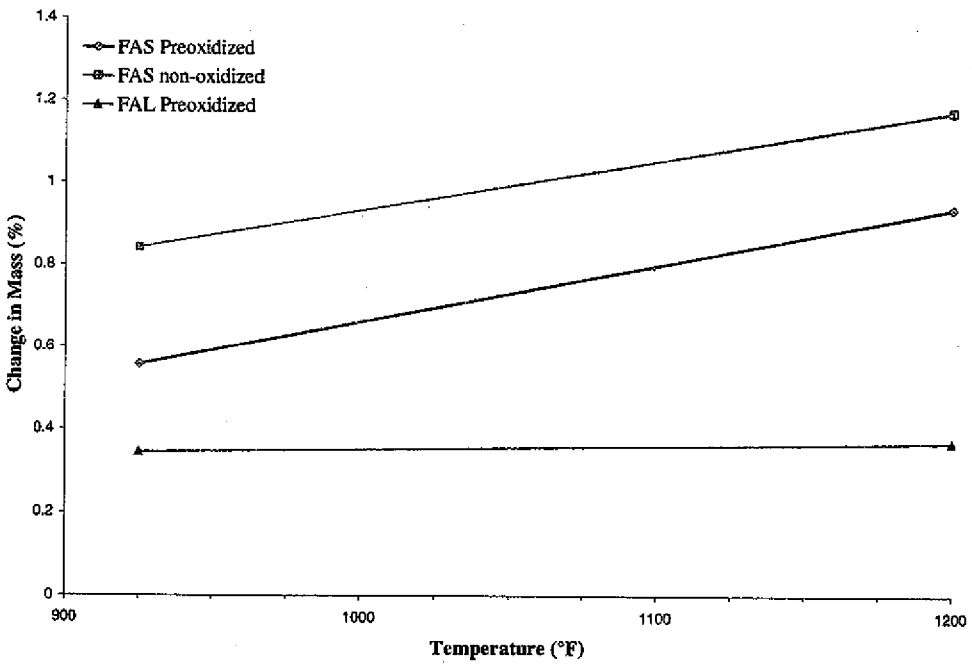

Figure 54: Change in mass versus exposure temperature with 0.783 vol% hydrogen sulfide.

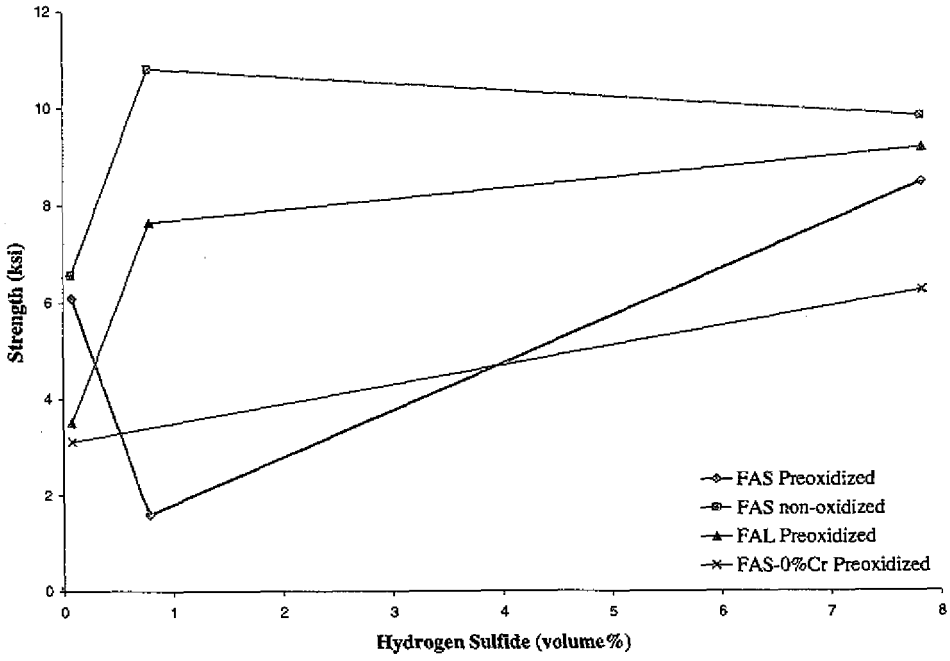

Figure 55: Strength versus hydrogen sulfide exposure level at 925°F. Strength tested by ring burst test.

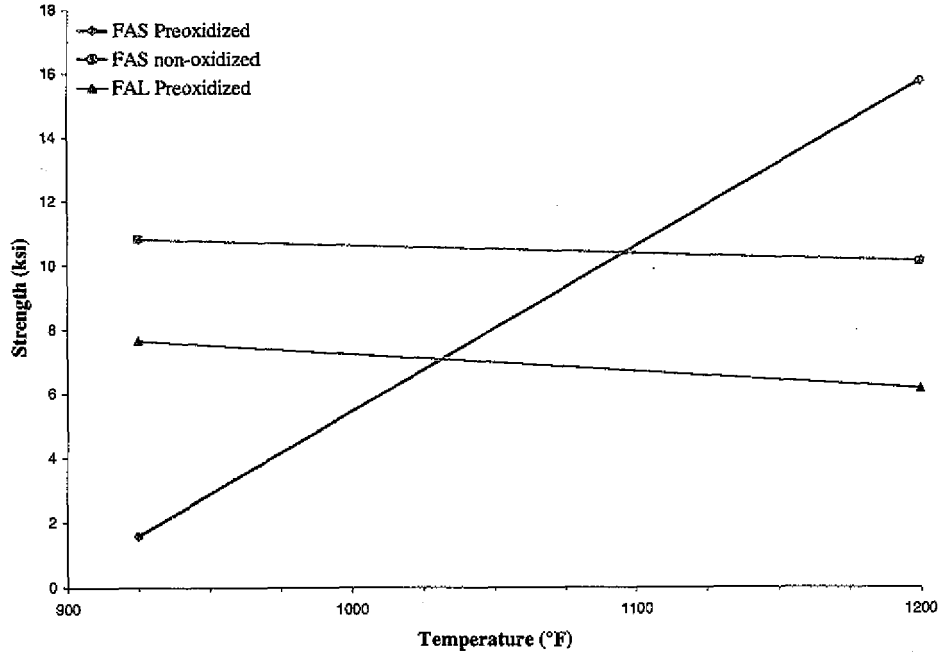

Figure 56: Strength versus exposure temperature with 0.783 vol% hydrogen sulfide. Strength tested with the ring burst test.

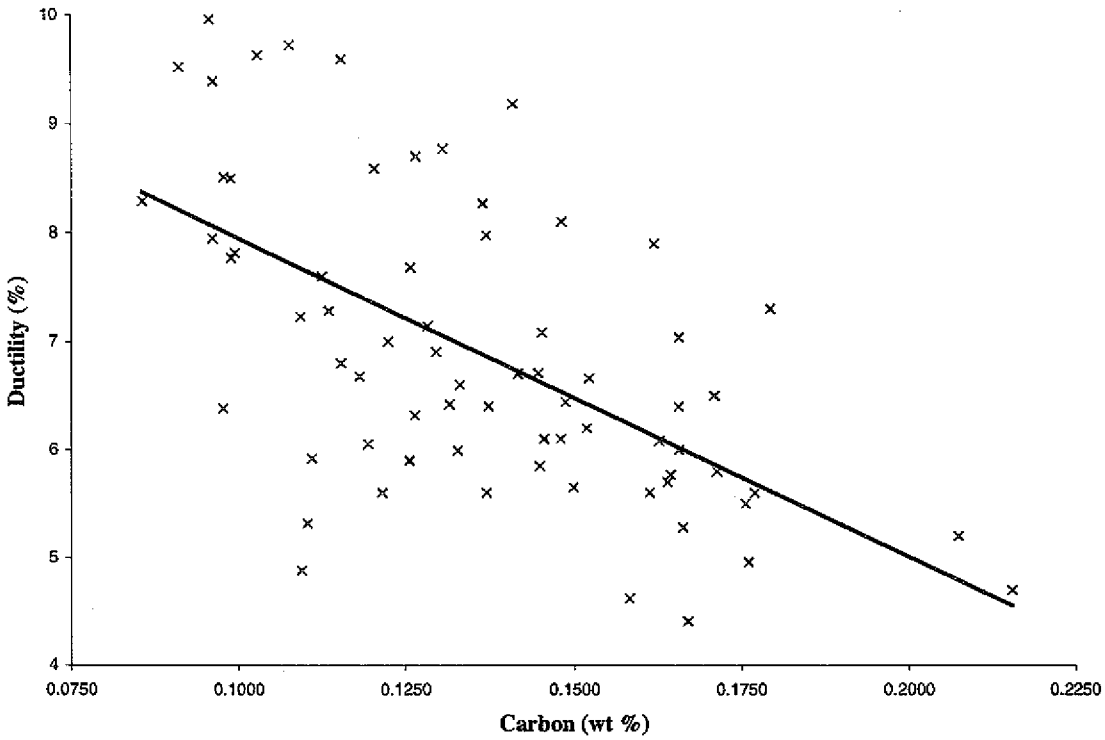

Figure 57: Ductility versus carbon content for as-sintered FAS media. Samples were prepared with varying binder concentrations and sintering in varying conditions. Decreasing the carbon content in the media increases ductility.